THESIS FOR THE DEGREE OF DOCTOR OF PHILOSOPHY

Stainless Steel Corrugated Web I-Girders for Composite Road Bridges

FATIMA HLAL

Department of Architecture and Civil Engineering
Division of Structural Engineering
Chalmers University of Technology
SE-412 96 Gothenburg, Sweden
Telephone: +46 (0)31 772 1000
www.chalmers.se

Cover illustration:
A composite road bridge with stainless steel corrugated web I-girders, highlighting the three areas under focus in this study.

Abstract

Achieving a sustainable bridge design requires a comprehensive evaluation of both economic feasibility and environmental impact throughout the structure's lifespan. While stainless steel is widely recognized for its superior life cycle performance, its high cost has limited its broader application in bridge construction. This thesis investigates a new design solution comprising stainless steel corrugated web I-girders for composite road bridges. This design solution is expected to reduce material usage and compensate for the higher cost of stainless steel, making it a more viable option for bridge girders.

The thesis is structured around three key areas of investigation. First, a comparative study is conducted to evaluate stainless-steel corrugated web girders against conventional carbon steel flat web girders. Second, the issue of flange buckling in stainless steel corrugated web I-girders is studied, noting that EN 1993-1-5 often yields unsafe predictions for carbon steel and has not been updated for stainless steel. Third, a fatigue assessment of the fatigue-prone welded detail between the corrugated web and the flange is conducted, noting that current design standards like EN 1993-1-9 do not categorize this detail, and that no fatigue test data exists for stainless steel.

In concept evaluation, two design solutions—carbon steel S355 with flat web and stainless steel EN1.4162 with corrugated web I-girders—are compared through parametric studies using a simply supported reference bridge. A design optimization tool employing genetic algorithm is developed and employed to optimize each design solution concerning weight, investment cost, life cycle cost (LCC), or environmental impact. The results showed that the new concept can be realized with a moderate increase in investment cost, bridging the cost gap between carbon and stainless steel, while offering lower life cycle costs and reduced climate impact compared to the traditional concept—particularly for bridges with deeper girders, higher average daily traffic, and more intense maintenance activities.

With reference to the flange buckling behaviour, a parametric finite element model is developed and validated. A linear buckling analysis (LBA) and geometrically and materially nonlinear analysis with imperfections (GMNIA) are carried out on 410 girders. The results are compared to previously developed models for carbon steel, and a buckling coefficient factor, together with a new buckling curve, is proposed.

The fatigue of the flange-to-web welded detail is examined through both numerical and experimental studies. Initially, critical load effects at the corrugation corner—the crack initiation location—are identified, including membrane stress and stresses due to transverse flange bending. Subsequently, the combination of these effects in fatigue design is discussed. Additionally, 86 fatigue test results on carbon steel corrugated web members are compiled and categorized by the corrugation

angle. Statistical analysis is conducted, and four detail categories (DCs) are proposed for carbon steel.

Finally, to assess the applicability of the proposed detail categories to duplex stainless steel, 15 stainless steel (EN 1.4162) beams with different corrugation angles were tested under cyclic loading. The cracking modes were documented, followed by a statistical analysis and comparison with carbon steel. The tested beams demonstrated fatigue strength comparable to their carbon steel counterparts. In addition, a fatigue assessment using the Hot Spot Stress (HSS) and Effective Notch Stress (ENS) approaches was conducted. The HSS method with DC100 and the ENS method with DC225, both based on the maximum principal stress, provided conservative estimates of the fatigue strength of the tested beams.

Sammanfattning

Att uppnå en hållbar brodesign kräver en omfattande utvärdering av både ekonomisk genomförbarhet och miljöpåverkan under hela brons livslängd. Medan rostfritt stål är erkänt för sin överlägsna livscykelprestanda, har dess höga kostnad begränsat dess bredare tillämpning inom brokonstruktion. Denna avhandling undersöker en ny designlösning som omfattar I-balkar av rostfritt stål med korrugerade liv. Denna designlösning förväntas minska materialanvändningen och kompensera för den högre kostnaden för rostfritt stål, vilket gör det till ett mer genomförbart alternativ för broar med I-balkar.

Avhandlingen är strukturerad kring tre centrala undersökningsområden. I det första området genomförs en jämförandestudie där den nya designlösningen jämförs med konventionella I-balkar i kolstål. I det andra området studeras flänsbuckling i stålbalkar med korrugerade liv med utgångspunkt i att föreskrifter i EN 1993-1-5 ger resultat på den osäkra sidan för balkar i kolstål samt att standarden inte har uppdaterats avseende flänsbuckling i rostfria I-balkar med korrugerade liv. I det tredje området genomförs en bedömning avseende utmattningshållfasthet av svetsdetaljen mellan livet och flänsen i I-balkar med korrugerade liv, med utgångspunkt i att svetsdetaljen inte finns kategoriserad i EN 1993-1-9, och att inga testdata finns för rostfritt stål.

I konceptutvärderingen jämförs två designlösningar— I-balkar i kolstål S355 med platt liv och I-balkar i duplex rostfritt stål EN1.4162 med korrugerade liv—genom parametriska studier med en fritt upplagd referensbro. En designoptimeringsfunktion som använder en genetisk algoritm utvecklas och används för att optimera varje designlösning med avseende på vikt, investeringskostnad, livscykelkostnad eller miljöpåverkan. Resultaten visade att det nya konceptet kan realiseras med en måttlig ökning av investeringskostnaden, vilket minskar kostnadsgapet mellan kolstål och rostfritt stål, samtidigt som det erbjuder lägre livscykelkostnader och minskad klimatpåverkan jämfört med det traditionella konceptet—särskilt för broar med djupare balkar, högre genomsnittligt trafikflöde och mer omfattande underhållsarbete.

Med hänvisning till flänsbucklingens beteende utvecklas och valideras en parametrisk finita elementmodell. En linjär bucklingsanalys (LBA) och geometriskt och materiellt icke-linjär analys med imperfektioner (GMNIA) genomförs på 410 balkar. Resultaten jämförs med tidigare utvecklade modeller för kolstål, och en bucklingskoefficientfaktor tillsammans med en ny bucklingskurva föreslås för flänsbuckling i I-balkar med korrugerade liv i duplex rostfritt stål.

Utmattningshållfasthet hos fläns-till-liv-svetsdetaljer undersöks genom både numeriska och experimentella studier. Kritiska belastningseffekter identifieras vid korrugeringshörnen (sprickinitieringsplatsen), inklusive membranspänning och flänsens

tvärgående böjning. Vidare diskuteras kombinationen av deras effekt i utmattningsdesign. Därefter sammanställs och analyseras 86 utmattningstestresultat på I-balkar av kolstål med korrugerade liv. Baserat på kategorisering av data avseende korrugeringsvinkel, föreslås fyra detaljkategorier. Avslutningsvis testas femton EN1.4162-balkar med varierande korrugeringsvinklar under cyklisk belastning för att bedöma tillämpligheten av dessa kategorier på duplex rostfritt stål. De observerade sprickmoderna dokumenteras. En statistisk analys genomförs, och resultaten jämförs med detaljkategorierna för kolstål. Testresultaten visade att duplex rostfritt stål med korrugerat liv uppvisade en jämförbar utmattningshållfasthet med kolstål. Resultaten analyserades även med hjälp av metoderna "Hot Spot Stress (HSS)" och "Effective Notch Stress (ENS)", båda baserade på den maximala huvudspänningen, vilka gav konservativa uppskattningar av utmattningshållfastheten hos de testade balkarna.

Nyckelord

Optimering, Genetisk algoritm, Investeringskostnad, LCC/LCA, Samverkansvägbroar, I-balkar med korrugerade liv, Duplex rostfritt stål, Flänsbuckling, Utmattningshållfasthet, HSS/ENS

Preface

The work presented in this thesis was carried out at Chalmers University of Technology, Department of Architecture and Civil Engineering, Division of Structural Engineering, between September 2021 and September 2025. It was conducted within the framework of two projects: *Sustainable and Maintenance-Free Bridges*, funded by Trafikverket (Project No. TRV 2020/117504), and *Material & Cost-Effective Optimized Steel Structures for Long Fatigue Life – LONGLIFE*, funded by VINNOVA (Project No. 2022–01614). Financial support and contributions from all our industrial partners are gratefully acknowledged. Special thanks are extended to Outokumpu, Borga, Swerim, COWI, and HiFIT for their valuable contributions to these projects.

I would like to thank my main supervisor, Professor Mohammad Al-Emrani, for his continuous support, guidance, encouragement, and much more throughout every stage of my PhD journey. My sincere thanks also go to my supervisors, Dr. Mozhdeh Amani, Dr. Peter Nilsson, and Dr. Jincheng Yang, for their valuable input, support, and belief in my work. I am also grateful to my examiner, Professor Holger Wallbaum, for his kindness and support.

To my colleagues at Chalmers and WSP, thank you for creating such a friendly and supportive environment. I'm especially grateful to Senior Research Engineers Anders Karlsson and Sebastian Almfeldt for their generous assistance during the experimental work, and to Docent Alexander Hollberg for his valuable guidance in the LCC/LCA analysis.

Finally, to my family and friends—thank you for your love and support. I am deeply grateful and wish you all the best in life.

Gothenburg, 2025
FATIMA HLAL

List of publications

This thesis is based on the following papers:

I.   **Hlal, F.**, Amani, M., & Al-Emrani, M. (2024). Stainless Steel Corrugated Web Girders for Composite Road Bridges: Optimization and Parametric Studies. *Engineering Structures* 302. https://doi.org/10.1016/j.engstruct.2023.117366

    Summary of the paper: This paper explores the feasibility of using stainless steel corrugated web I-girders as an alternative to traditional carbon steel flat web girders in composite road bridges. This design solution is anticipated to reduce investment costs, thereby facilitating a wider application of the advantageous properties provided by stainless steel. The findings indicated that the concept can narrow the investment cost gap between carbon and stainless steel while offering significant potential for LCC savings and reduced environmental impact for the analysed span lengths, particularly in scenarios involving deeper girders, high average daily traffic (ADT), and more intensive maintenance activities.
    Author's contribution: The author of this thesis is the corresponding author. She contributed to the development of the design optimization tool, the selection of studied design parameters, and the analysis of the data. Additionally, she was responsible for visualizing the results, drafting the original manuscript, and conducting the review and editing process.

II.   **Hlal, F.**, & Al-Emrani, M. (2023). Flange Buckling in Stainless-Steel Corrugated Webs I-Girders under Pure Bending: Numerical Study. *Journal of Constructional Steel Research,* 208. https://doi.org/10.1016/j.jcsr.2023.108031

    Summary of the paper: This study examines flange buckling in duplex stainless-steel corrugated web I-girders. Previous research has shown that the current EN1993–1-5 design model often overestimates flange buckling capacity and is only applicable to carbon steel. In this work, both parametric linear buckling analysis (LBA) and geometrically and materially nonlinear analysis with imperfections (GMNIA) were carried out. Based on the results, a new buckling curve and design procedure are proposed for duplex corrugated web I-girders.
    Author's contribution: The corresponding author conducted the literature review and contributed to the development of the methodology and selection of parameters. She also participated in the numerical analysis, FE model validation, Python scripting of the parametric model, data analysis, results visualization, manuscript preparation, and the review and editing process.

III.   **Hlal, F.**, & Al-Emrani, M. (2024). Load effects in beams with corrugated webs: Numerical study. *Nordic Steel Construction Conference 2024, Luleå, Sweden. The Swedish Institute of Steel Construction.* https://doi.org/10.5281/zenodo.12210008

   Summary of the paper: This study uses finite element analysis to examine the effects of membrane and transverse bending on stress magnitudes at corrugation corners, which are typical crack initiation locations. Transverse bending is found to increase stress at specific locations, making them more susceptible to fatigue cracking, highlighting the need to account for its effects in fatigue design.
   Author's contribution: The corresponding author's contribution includes methodology, numerical analysis, results analysis, results visualization, and manuscript preparation, including both the original draft and review & editing.

IV.   **Hlal, F.**, & Al-Emrani, M. (2025). Load effects for fatigue design of web-to-flange welded detail in corrugated web girders. *SEMC 2025: The Ninth International Conference on Structural Engineering, Mechanics and Computation, Cape Town, South Africa. Engineering Materials, Structures, Systems and Methods for a More Sustainable Future.* CRC Press. https://doi.org/10.1201/9781003488644-79

   Summary of the paper: Building on the load effects identified in the previous paper, this study combines experimental testing and finite element analysis to examine their influence on stress concentrations at crack initiation locations, with a focus on hot-spot stresses. Transverse bending is found to exhibit stress concentration factors similar to those of membrane stress, supporting their superposition in fatigue design using S-N curves derived in settings that do not involve significant transverse bending.
   Author's contribution: The corresponding author's contributions include participating in the methodology, conducting numerical analyses, planning and participating in the experimental work, processing and visualizing the data, and drafting the manuscript.

V.   **Hlal, F.**, & Al-Emrani, M. (2025). Detail categories for the flange-to-web weld detail in corrugated web girders. *Engineering Structures* 324. https://doi.org/10.1016/j.engstruct.2024.119342

   Summary of the paper: In this paper, the authors compiled and analysed 86 fatigue test results on members with corrugated webs sourced from literature. Based on the findings, four fatigue detail categories (DC) were proposed, classified according to the corrugation angle. Furthermore, the study employed effective notch stress (ENS) analysis to assess the applicability of DC225, as recommended by the International Institute of Welding (IIW) for the examined detail. The thickness effect, as well as toe and root cracking, are also discussed.

Author's contribution: The corresponding author's contributions include conducting the literature review and contributing to the methodology, data curation, and data analysis. The author was also responsible for carrying out the numerical analysis, visualizing the results, and preparing the manuscript.

VI.   **Hlal, F.**, & Al-Emrani, M. (2025). Experimental and Numerical Fatigue Assessment of Duplex Stainless-Steel Corrugated Web I-Girders. *Manuscript under revision in Engineering Structures.*

Summary of the paper: In this paper, an experimental study on 13 duplex stainless-steel (EN 1.4162) beams with varying corrugation angles and radii is reported. Cracking modes, including web and flange cracking, are documented, and statistical analysis is carried out. The results indicated fatigue strength equivalent to that of carbon steel. Moreover, fatigue assessments using the DC100 and DC255 categories with the HSS and ENS methods, according to IIW, produced conservative results for the tested beams.

Author's contribution: The corresponding author contributed to the test specimens design, planning, and participation in the experimental work, numerical analysis, data post-processing, visualization of results, and manuscript preparation.

Additional contributions from the author

- **Hlal, F.**, Al-Emrani, M., & Amani, M. (2022). Preliminary study on plate girders with corrugated webs. *Report ACE 2022:3. Chalmers University of Technology*.
  https://research.chalmers.se/publication/530413

- Al-Emrani, M., Amani, M., Björnstedt, P., Borg, P., Forsgren, E., Hedegård, J., Hällmark, R., **Hlal, F.**, Janiak, P., Lundstjälk, A., Nilsson, P., Persson, L., Trydell, K., Zachrisson, J., & Zamiri, F. (2022) SUNLIGHT – Sustainable, maintenance-free and lighter beams for stronger Swedish infrastructure.

- **Hlal, F**., Amani, M., Nilsson, P., Hollberg, A., & Al-Emrani, M. (2023) Life cycle cost and life cycle assessment of composite bridge with flat and corrugated webs. *CE/Papers*, 6(3-4), 574-579. https://doi.org/10.1002/cepa.2514

- Al-Emrani, M., & **Hlal, F.** (2025). Fatigue strength of flange-to-web welded detail in corrugated web girders. *SEMC 2025: The Ninth International Conference on Structural Engineering, Mechanics and Computation, Cape Town, South Africa. Engineering Materials, Structures, Systems and Methods for a More Sustainable Future.* CRC Press.
  https://doi.org/10.1201/9781003677895-74

Licentiate thesis

- **Hlal, F.** (2023). Stainless Steel Corrugated Web Girders for Composite Road Bridges. *Technical Report ACE 2023:9. Chalmers University of Technology*.
  https://research.chalmers.se/publication/536891

Master thesis

- **Hlal, F.**, & Mohra, N. (2021). Shear behaviour and imperfection sensitivity analysis of Stainless-Steel girders with corrugated web plates. *Chalmers University of Technology*.
  Available at: https://odr.chalmers.se/

Nomenclature and Acronyms

Below is the nomenclature of variables that have been used throughout this thesis:

α [deg]	Corrugation angle
R [mm]	Corrugation bend radius
a_1 [mm]	Length of flat fold
a_2 [mm]	Length of inclined fold
a_3 [mm]	Corrugation depth
a_4 [mm]	Length of inclined fold projection on longitudinal axis
f_y [MPa]	Yield strength
f_u [MPa]	Ultimate tensile strength
t_f [mm]	Flange thickness
b_f [mm]	Flange width
c_f [mm]	The larger outstand of the flange
t_w [mm]	Web thickness
h_w [mm]	Web height
a_w [mm]	Fillet weld throat thickness
δ [mm]	Out-of-plane deflection
r [mm]	Effective notch radius
σ [MPa]	Stress
σ_{cr} [MPa]	Elastic buckling stress
σ_E [MPa]	Elastic buckling stress (Euler theory)
$\sigma_{x.m}$ [MPa]	Membrane stress in X-direction
$\sigma_{x.b}$ [MPa]	Bending stress in X-direction
σ_t [MPa]	Transverse bending stress
$\Delta\sigma_{nom}$ [MPa]	Nominal stress range
σ_{hs} [MPa]	Hot spot stress
ENS_{Toe} [MPa]	Effective notch stress at the weld toe
ENS_{Root} [MPa]	Effective notch stress at the weld root
SCF_{Toe} [−]	Stress concentration factor at the weld toe
χ [−]	Reduction factor for out-of-plane buckling

$\rho \ [-]$	Flange buckling reduction factor
$k_\sigma \ [-]$	Elastic buckling coefficient
$v \ [-]$	Poisson's ratio
$\overline{\lambda_p}[-]$	Relative slenderness
$\kappa_{\sigma.corr} \ [-]$	Proposed elastic buckling coefficient
$\rho_{corr} \ [-]$	Proposed buckling reduction factor of plate width
$M_{ult.\ Corr} \ [kNm]$	Moment capacity with reference to flange buckling
$V \ [kN]$	Shear force
$M_z \ [kNm]$	Transverse bending moment
$M_y \ [kNm]$	Bending moment around the y-axis
$I_y \ [mm^4]$	Second moment of area around the y-axis
$I_z \ [mm^4]$	Second moment of area around the z-axis
Mult [kNm]	Ultimate moment capacity from FEA
Mpl [kNm]	Plastic moment capacity
$f_T(M_z) \ [-]$	Reduction factor due to transverse bending
N [cycles]	Number of cycles to failure

Below is the list of acronyms that have been used throughout this thesis, listed in alphabetical order:

ADT	Average daily traffic
B-point	Initiation points of web fatigue cracks at the web weld toe
CSC4	Cross-section class 4
CWG	Corrugated web girder
CWT	Corrugated web T-section member
DC	Detail category
DC100	Detail category 100
DC225	Detail category 225
ENS	Effective notch stress
EPD	Environmental product declaration
FEA	Finite element analysis
FLS	Fatigue limit state
GMNIA	Geometrically and materially nonlinear analysis with imperfections

HFs	Horizontal folds (or flat folds)
HSS	Hot spot stress
IFs	Inclined folds
IIW	International Institute of Welding
LBA	Linear buckling analysis
LCA	Life cycle assessment
LCC	Life cycle cost
MPC	Multi-point constraint
N_{obs}	Number of heavy vehicles per slow lane
S-point	Initiation points of flange fatigue cracks at the flange weld toe
SCF	Stress concentration factor
SLS	Serviceability limit state
ULS	Ultimate limit state

Contents

Part 1 – Extended Summary

Chapter 1

1 Introduction

1.1 Background

Sustainable development is now a key focus for businesses and governments. In 2015, the United Nations introduced the 2030 Agenda for Sustainable Development [1], which includes 17 goals. The European Union [2] is also committed to sustainability with its "Next Steps for a Sustainable European Future" initiative. This framework emphasizes the integration of social, environmental, and economic concerns in all policies.

Infrastructure such as bridges can contribute to sustainable development by ensuring cost-effectiveness throughout their entire lifecycle, from construction to decommissioning, while also minimizing user disruptions during construction and maintenance [3]. Bridges also play a social role by prioritizing the well-being of both construction workers and surrounding communities. Environmentally, bridges contribute to sustainable development by minimizing carbon dioxide emissions and embodied energy during fabrication and construction. Additionally, incorporating recyclable and reusable components at the end of a bridge's lifespan further enhances sustainability.

A twin I-girder steel-concrete composite bridge is a common design alternative for road bridges in Europe [4]. The bridge girders are typically made of carbon steel with flat webs and are connected to a concrete deck using shear studs, enabling efficient material use through composite action [5]. However, carbon steel is prone to corrosion, requiring costly protective coatings and frequent maintenance, which can cause environmental impact and traffic disruptions [6]. To mitigate these challenges, stainless steel, particularly duplex stainless steel, offers a viable alternative due to its superior strength, corrosion resistance, and durability [3, 7]. Several studies have highlighted the potential savings in life-cycle costs (LCC) [8] [9] [10] and life cycle impact [10] that can be achieved by using stainless steel. Despite its long-term benefits and superior structural properties, stainless steel has limited use in bridge construction, primarily due to its higher initial investment costs compared to conventional carbon steel. For instance, the cost of stainless steel is around 3-5 times that of carbon steel S355 per kilogram, which contributes to this disparity [6].

In conventional girder designs with flat webs (Figure 1a), increasing girder depth enhances shear and bending resistance. However, ensuring stability typically requires either thicker webs to reduce slenderness or additional stiffeners. These adjustments increase material consumption and production costs and introduce more fatigue-prone details. Alternatively, girders with corrugated webs (Figure 1b) can meet the required shear capacity using significantly thinner plates, eliminating the need for additional transverse stiffeners and enabling substantial savings in material usage [6].
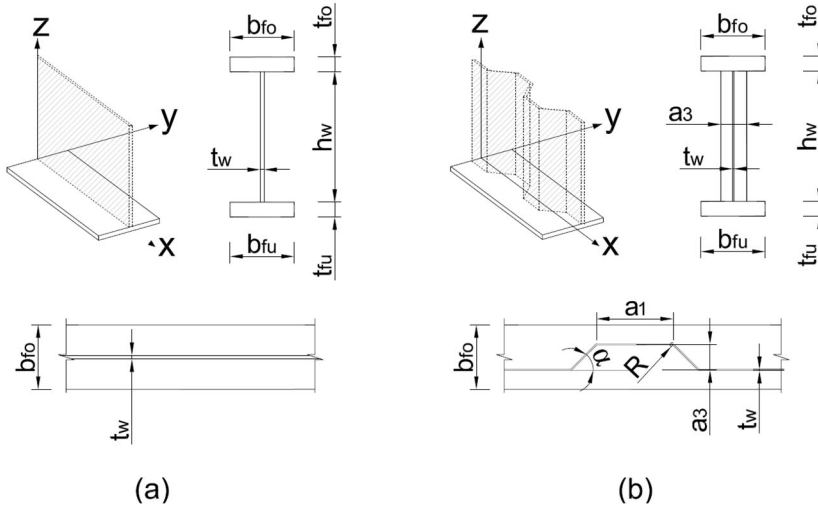

Figure 1 Composite bridge girder: (a) with flat web (b) with corrugated web

The investigations of using corrugated steel webs as a substitute for stiffened webs in steel-girder bridges started in Japan in 1965 [11], and in the 1980s, France constructed the first box-girder composite bridge featuring corrugated steel webs along with upper and lower concrete slabs, leading to the development of multiple composite bridges in the country [11]. Japan further advanced this concept in the 1990s by developing corrugated-web precast box-girder bridges, with over 140 bridges constructed by 2015 [11]. With reference to twin I-girder bridges, the only known corrugated-web I-girder bridge was built in the United States in 2005 in Bradford County, Pennsylvania, as a demonstration project, showcasing trapezoidal corrugated webs and constructed using High-Performance Weathering Steel (HPS 70W)[12].

Incorporating corrugated webs in stainless steel bridge I-girders can offer a cost-effective design solution that helps bridge the material cost gap between stainless and carbon steel girders by reducing material usage. A preliminary study conducted by Wahlsten et al. [6] indicated notable potential savings in material and life cycle costs by using stainless steel corrugated web I-girders as an alternative to carbon steel flat web I-girders. However, the study, as well as most previous studies

interested in evaluating the use of stainless steel for road bridges [6] [8] [9] [13], compared stainless and carbon steel by only changing materials while keeping other design parameters constant. This may —of course — not provide the best insight into the potential of using stainless steel. The difference in material cost may, for example, render other design solutions to be more economical (e.g., girder dimensions and system layout). Therefore, further research is needed to explore optimal designs across various concepts, accounting for different design parameters— such as span length, allowable girder height— that could influence the design before reaching general conclusions about this design's potential.

For safe design of stainless-steel I-girders with corrugated web, a design procedure should be established. Annex D of EN1993-1-5 provides design rules for corrugated web beams; however, these guidelines are based on carbon steel and have not been updated for stainless steel. Currently, the rules in Eurocode focus solely on bending moment capacity and shear resistance. The shear capacity of duplex corrugated web beams was investigated in the SUNLIGHT project at Chalmers, revealing that the use of stainless steel for beams with intermediate slenderness can yield higher shear strength [14]. However, previous studies have shown that applying the EN 1993-1-5 model for flange buckling—which influences the bending moment capacity—can lead to unsafe resistance predictions for carbon steel girders [15]. The basis of this model is detailed in the Commentary and Worked Examples to EN 1993-1-5 [16]. The applicability of this model to stainless steel is also uncertain, suggesting a need for further research and potentially the development of a new model tailored to stainless steel.

To employ these beams as bridge girders, it is essential to assess their fatigue strength. Currently, EN 1993-1-9 [17], as well as a draft for its new version [18], does not provide a specific detail category (DC) for the fatigue design of flange-to-web welded details in beams with corrugated webs, whether made of carbon or stainless steel. Therefore, establishing DCs for both materials is needed. Furthermore, the distinctive geometry of corrugated webs has been shown to significantly affect the stress distribution within the girder flanges [19, 20], making it critical to identify the relevant stress components for fatigue design. Multiple fatigue experiments on carbon steel members with corrugated webs have been conducted and reported in the literature [21-28]. These include beams subjected to four-point and three-point bending, as well as T-section tension members composed of a flange plate and a welded corrugated web. These test data with different corrugation geometries form a database that can be used to establish detail categories (DCs) for carbon steel girders. However, comparable experimental data for stainless steel girders are currently lacking. Therefore, an experimental program is needed to evaluate the fatigue strength of stainless-steel girders.
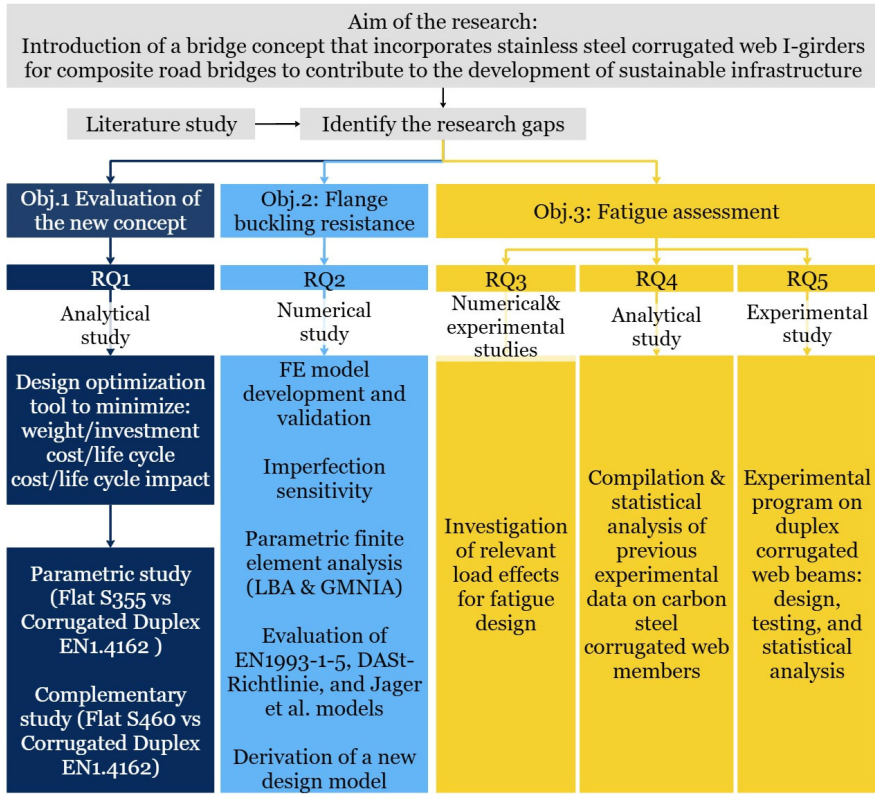
1.2 Aim and objectives

The overall aim of this thesis is to contribute to the development of sustainable infrastructure by making the benefits offered by stainless steel more attainable in the construction of road bridges. This is achieved through the introduction of a bridge concept that incorporates stainless steel corrugated web I-girders for composite road bridges. This concept is expected to reduce the investment cost gap between carbon and stainless steel while also generating lower environmental impact and life cycle cost. Moreover, to support the implementation of this concept, a basis for designing stainless steel corrugated web girders needs to be established. The literature review highlighted flange buckling and fatigue assessment as the primary design aspects that need to be addressed. Within this overall aim, the following main objectives are defined and covered in this thesis:

1. Evaluate the design concept, focusing on:
   - RQ1: How does the studied design concept of duplex stainless-steel corrugated web girders compare to conventional carbon steel flat web girders in terms of weight, investment cost, life-cycle cost, and environmental impact, and how does its viability vary with different design inputs such as span length, girder depth, average daily traffic (ADT), and maintenance intervals?
2. Develop a prediction model for flange buckling in stainless steel corrugated web beams, focusing on:
   - RQ2: How do the existing models in current standards and literature—originally developed for carbon steel—perform when applied to duplex stainless-steel girders? What alternative model can be proposed, and what is an appropriate classification limit for Class 4 cross-sections in these elements?
3. Provide a basis for fatigue verification of the flange-to-web welded detail in corrugated web beams, with a focus on the following questions:
   - RQ3: What are the load effects that need to be considered in fatigue design, and how should they be combined?
   - RQ4: How do the corrugation geometrical parameters, such as the corrugation angle and bend radius, affect the fatigue strength of the studied detail? What S–N curves or detail categories can be proposed based on these parameters?
   - RQ5: How does the fatigue performance of this detail in duplex stainless-steel compare with that in carbon steel?

1.3 Methodology

A schematic illustration of the methodological approaches used in this thesis is presented in Figure 2.

Aim of the research:
Introduction of a bridge concept that incorporates stainless steel corrugated web I-girders for composite road bridges to contribute to the development of sustainable infrastructure

Literature study → Identify the research gaps

Obj.1 Evaluation of the new concept	Obj.2: Flange buckling resistance	Obj.3: Fatigue assessment		
RQ1	RQ2	RQ3	RQ4	RQ5
Analytical study	Numerical study	Numerical& experimental studies	Analytical study	Experimental study
Design optimization tool to minimize: weight/investment cost/life cycle cost/life cycle impact	FE model development and validation

Imperfection sensitivity

Parametric finite element analysis (LBA & GMNIA)

Evaluation of EN1993-1-5, DASt-Richtlinie, and Jager et al. models

Derivation of a new design model | Investigation of relevant load effects for fatigue design | Compilation & statistical analysis of previous experimental data on carbon steel corrugated web members | Experimental program on duplex corrugated web beams: design, testing, and statistical analysis |
| Parametric study (Flat S355 vs Corrugated Duplex EN1.4162)

Complementary study (Flat S460 vs Corrugated Duplex EN1.4162) | | | | |

Figure 2 Overview of the methodological approach

The first part of this research was focused on evaluating the concept of stainless-steel corrugated web I-girders as a sustainable solution in twin I-girders composite bridges. Given the variability of design inputs across bridge projects, a Python-based design optimization tool employing a Genetic Algorithm has been developed and employed to conduct a series of parametric studies using a simply supported reference bridge. The optimization tool can optimize the design with respect to weight, investment cost, LCC, or environmental impact. The study compares optimal design solutions for two primary girder alternatives: conventional S355 flat web girders, commonly used in practice [3], and corrugated web girders made of lean duplex stainless steel EN 1.4162. The latter has been more often considered for its high strength and lower cost due to its low nickel content compared to standard duplex [29], and is increasingly used in welded structures exposed to corrosive environments as a good alternative to carbon steel [30]. The comparison is conducted with reference to weight, investment cost, life cycle cost, and life cycle environmental impact, with focus on the saving of LCC achieved for different design inputs. Additionally, a supplementary comparison between S460 flat web girders and EN 1.4162 corrugated web girders is carried out to provide further insights, given the closer strength alignment between these two materials.

Thereafter, the flange buckling problem is investigated through parametric geometric and materially non-linear analysis with imperfections (GMNIA). This method considers both material and geometric non-linearities and has been proven to provide—compared to experiments— realistic and accurate prediction of how structures behave under load [31] [32] [33]. The study is conducted on 410 girders with dimensions representative of bridge girders. A sensitivity analysis of initial imperfections is conducted on duplex EN1.4162 and compared to established imperfection sensitivity curves for carbon steel to determine an appropriate equivalent initial imperfection based on eigenmode scaling. The numerical results are then compared to existing design models in the Eurocode standard and the DASt-Richtlinie 015 [34] as well as to other design models proposed previously for carbon steel girders.

With reference to fatigue assessment, the load effects that are relevant for fatigue design and the combination of these effects are investigated using finite element analysis and experimental work. Consequently, 86 fatigue test results reported in the literature are compiled, evaluated, and categorized based on the corrugation angle, which has been identified as the most significant geometric parameter in previous studies. Finally, a fatigue testing program on 15 duplex EN1.4162 beams is conducted. The goal is to verify the fatigue strength of the detail in stainless steel and compare it to the data collected on carbon steel. The test program included two series of beams with varying corrugation angles and radii, enabling comparison with corresponding data from the literature on carbon steel.

1.4 Limitations

- This thesis focuses exclusively on the lean duplex stainless steel (EN 1.4162) in concept evaluation, flange buckling resistance, and fatigue testing program. This type of stainless steel has good weldability and contains less nickel, making it much cheaper than austenitic and standard duplex grades [30]. Its cost is roughly 30–40% lower than that of austenitic and standard duplex grades.
- The developed optimization routine focuses exclusively on the steel part of the bridge superstructure, including the main girders' dimensions, corrugation parameters, and the spacing between cross bracings. The concrete deck and the center-to-center distance between the two main girders are not optimized.
- In evaluating the design concept across varying input parameters, only two steel types were considered —S355 carbon steel and EN 1.4162 stainless steel. A supplementary study on S460 was also conducted. The tool, however, is designed to incorporate more steel grades and types, such as weathering steel, for the possibility of future studies.
- Material prices and EPDs were sourced from one Swedish producer per steel type, and the production cost calculation model

is based on 2022 market prices from two Swedish manufacturers. As these values fluctuate over time and between producers, the results may change depending on the input data.

- The developed model for flange buckling was based on pure bending conditions; additional stresses arising from shear flow were not considered.
- This thesis includes a fatigue assessment of the flange-to-web welded detail in trapezoidal corrugated web beams, which leads to flange fatigue cracking. While web fatigue cracking is noted, it is not investigated thoroughly in this work.

1.5 Original features

The original features of the present work are summarized below:

- In **Paper I,** it was demonstrated that the concept of stainless-steel corrugated web girders offers a promising solution for road bridge girders. Depending on the design input, this approach can reduce the cost disparity between stainless steel and carbon steel, while still preserving the long-term benefits inherent to stainless steel, including corrosion resistance and low maintenance requirements.
- In **Paper II**, a new design model has been developed for the flange buckling resistance of duplex EN1.4162 corrugated web beams, incorporating a relative slenderness limit for CSC4.
- **Paper III and IV** provide an understanding of the various load effects acting on the flanges of corrugated web girders, their influence on crack initiation locations, and how to combine these effects in fatigue design.
- In **Paper V,** four distinct detail categories based on the corrugation angle were proposed. Additionally, the applicability of the Effective Notch Stress (ENS) method for the studied detail was evaluated.
- In **Paper VI,** fatigue testing was conducted on beams with corrugated webs made of EN1.4162. To the author's knowledge, this is the first study to investigate fatigue behaviour of duplex stainless steel corrugated web beams.

1.6 Outlines

- Chapter 1 presents the background of the work and introduces its aim, objectives, methods, limitations, and original features.
- Chapter 2 provides the knowledge required to establish the theoretical framework.
- Chapter 3 provides an overview of the studies conducted in this research and summarizes the main results and findings across the appended publications.
- Chapter 4 presents the main conclusions drawn from this research work and gives suggestions for future research.

Chapter 2

2 Theoretical Background

This chapter presents the theoretical background relevant to the research. It begins with an overview of the structural behaviour of corrugated web beams, highlighting their unique characteristics. The following section presents the use of duplex stainless steel in bridge applications, outlining its advantages and suitability. Next, the principles of genetic algorithm optimization are introduced, with an explanation of its mechanism and relevance to the current study. The chapter concludes with a brief overview of Life Cycle Cost (LCC) and Life Cycle Assessment (LCA) methodologies in the context of bridge applications.

2.1 Structural behaviour of corrugated web beams

The geometric parameters that define a corrugated web beam include the corrugation angle (α), the bend radius (R), the corrugation depth (a_3), and the lengths of the flat (a_1) and inclined folds (a_2), as illustrated in Figure 3.
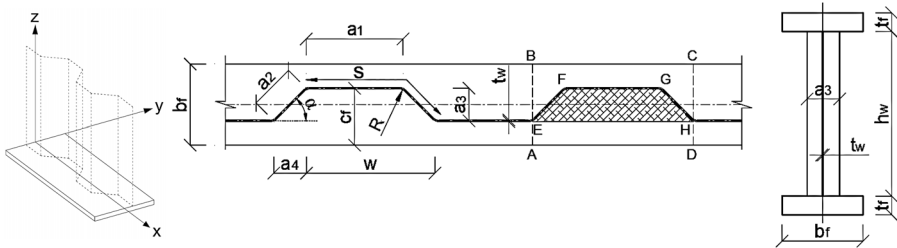
Figure 3 Geometrical parameters of girders with corrugated webs

The use of corrugated webs is primarily justified by their enhanced shear capacity and material saving compared to conventional flat web girders, which typically require longitudinal and/or transverse stiffeners in deep girder designs. In an experimental study conducted by Leblouba et al. [35], the corrugated web beam achieved a shear strength approximately 1.6 times greater than that of the flat web beam with similar dimensions.

In addition to enhancing shear buckling capacity, the unique geometry of corrugated webs significantly influences the overall structural behaviour of the beam. It alters the stress distribution between the web and flanges, affects the stress distribution within the flanges, and affects the buckling behaviour of the flange plates. Additionally, the corrugation geometry introduces stress concentrations at the corners of the folds, creating a fatigue-prone welded detail. Corrugated webs also affect the beam's resistance to lateral-torsional buckling and its response to localized loading, such as patch loading.

These key differences in structural behavior associated with corrugated web girders are discussed further in the following sections.

Accordion effect

Corrugated web beams exhibit inherently lower bending stiffness due to the web's folded geometry—a phenomenon commonly referred to as the "accordion effect". This characteristic significantly affects their structural behaviour under axial and bending loading. Consequently, when designing beams with corrugated webs, it is common to assume that the flanges primarily resist bending moments while the web resists the shear force [36]. Many studies on the bending behaviour of corrugated web I-girders have shown that normal stresses in the web are generally negligible, except in areas near and restrained by the flange plates [19] [37].

Research conducted by Inaam et al. [38] suggests that the web can contribute to bending resistance through what they term the "Web Participation Factor". They propose that designers consider a minimum contribution of 10% (or $0.1 * tw$) when evaluating the moment resistance of trapezoidal corrugated web beams under specific geometric conditions.

Transverse bending

In corrugated web beams, the shear flow between the web and the flange follows the corrugated web's profile, inducing transverse bending within the plane of the flanges (Figure 4) and consequently generating torsional effects throughout the section. This behaviour stems from the fold's eccentricity relative to the x-axis, which alters the shear flow at the flange-to-web junction, leading to additional transverse bending moments around the flange's strong axis (M_z in Figure 4). As a result, these induced bending stresses are superimposed on the existing normal stresses from primary bending (i.e., My), further influencing the overall structural response of the beam [19] [39] [20].
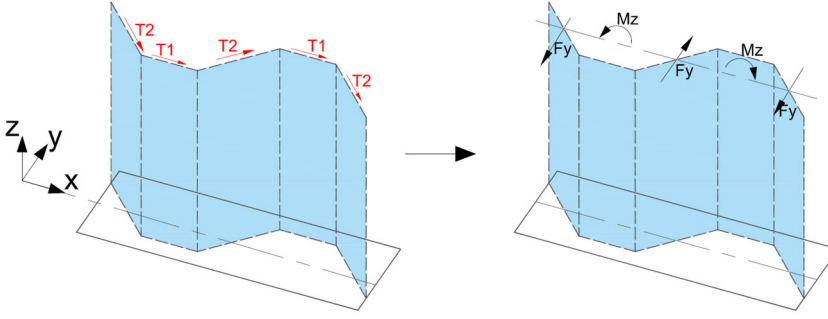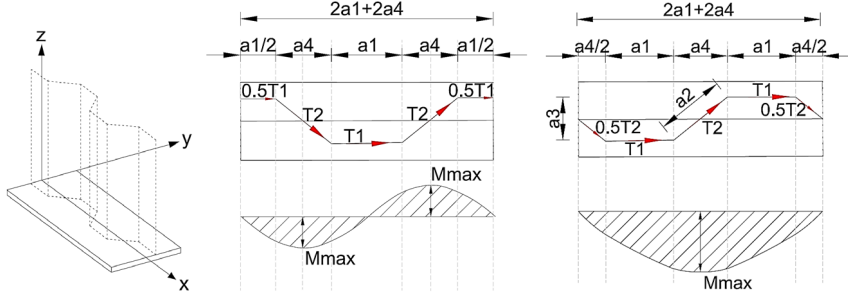
Figure 4 Transverse bending due to shear flow

Abbas et al. [40] proposed that analysing the out-of-plane behaviour of corrugated web beams in bending involves translating the shear flow at the flange-to-web intersection into equivalent external loads on the flange, i.e., the normal stresses (σ_x) in the flanges result from the superposition of in-plane and transverse flexural stresses about the y- and z-axes, as expressed in Equation (2-1).

$$\sigma_x = \frac{M_y \cdot z}{I_y} + \frac{M_z \cdot y}{I_z} \qquad (2\text{-}1)$$

Where z and y are the vertical and transverse distances from the neutral axes, while M_y, I_y, M_z, and I_z denote the bending moments and second moments of area around the y- and z-axes, respectively (Figure 5). I_y applies to the entire girder, while I_z applies to the flange.

EN1993-1-5 [41] takes into account the effect of this transverse bending moment by decreasing the yield strength of the flange by a factor $f_T(M_z)$ for both tension and compression flanges. This reduction is dependent on the magnitude of transverse bending stress caused by shear flow in the flanges. Regarding the magnitude of this transverse bending M_z, Baláž and Koleková [42] proposed the formula— given in Figure 5a— for calculating the maximum transverse moment based on two cases studied. Kövesdi et al. [39] later conducted a comprehensive investigation of various factors, including geometric properties and loading conditions, to determine the worst-case scenario for maximum additional normal stress on the flange due to shear flow. Their findings revealed that the maximum transverse moment was double that from Baláž and Koleková's earlier study (Figure 5b).

$$(a) \; M_{z.max} = \frac{V \cdot a_3}{4 \cdot h_w} \cdot (2 \cdot a_1 + a_4) \quad (b) \; M_{z.max} = \frac{V \cdot a_3}{2 \cdot h_w} \cdot (2 \cdot a_1 + a_4)$$

Figure 5 Transverse bending due to shear flow [19]. (a) Load and support positioned on the flat fold; (b) load and support positioned on the inclined fold. $M_{z.max}$ denotes the maximum transverse bending moment, and V represents the shear force. Refer to Figure 3 for the notations

Regarding the moment-shear (M-V) interaction, Kövesdi et al. [39] noted that the current proposal in EN1993-1-5 for the reduction factor $f_T(M_z)$ results in a conservative design, and the resistance reduction is not larger than other contributions typically neglected in the design of corrugated web girders, such as web contribution to bending resistance and flange contribution to shear resistance. Therefore, they concluded that the check for M-V interaction could be neglected in practical design when a plastic design method is applied. Moreover, Elgaaly et al. [33] [37] investigated the bending and shear behaviour of trapezoidal corrugated web girders. The researchers reported that there is no interaction between the bending and shear in trapezoidal corrugated web girders.

In a more recent study in 2022, Elamary et al. [32] investigated the behaviour of corrugated web beams subjected to bending and shear, using both experimental and numerical methods, with a focus on flanges classified as CSC4. This study specifically examines the influence of the loading position (i.e., whether the load is applied over horizontal folds (HFs) or inclined folds (IFs)) on the ultimate moment capacity. The authors concluded that the EN 1993-1-5 model is applicable for calculating the bending capacities of beams loaded on an inclined fold. However, they introduced a new formula for determining the bending capacity when the load is applied to the flat fold, which is expected to lead to a higher bending capacity.
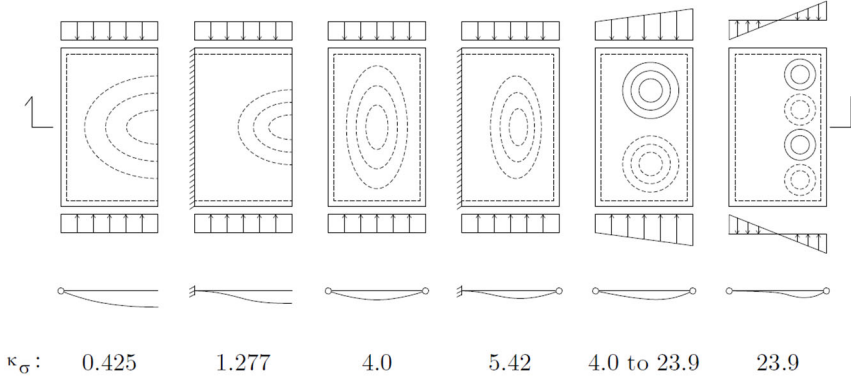
Flange plate buckling
In the context of plate buckling under axial loading, the elastic critical stress (σ_{cr}) and elastic buckling coefficient (k_σ) are fundamental parameters. The slenderness of a plate under a given axial load and boundary conditions is determined by calculating σ_{cr}, leading to the

derivation of the plate relative slenderness $\overline{\lambda_p} = \sqrt{f_y / \sigma_{cr}}$. This parameter indicates whether the plate under axial compression will buckle, necessitating a reduction in its effective width through the buckling reduction factor (ρ) (plates in cross-section class 4 [41]).

The elastic buckling stress is defined as $\sigma_{cr} = \sigma_E * k_\sigma$ where σ_E is the elastic buckling stress of a plate strut according to Euler's theory [43], Equation (2-2).

$$\sigma_{cr} = \sigma_E * k_\sigma, \ \sigma_E = \frac{\pi^2 E t^2}{12(1 - v^2) b^2} \tag{2-2}$$

Where b and t are the width and the thickness of the plate, v is Poisson's ratio. The boundary conditions and the loading conditions are then considered through the elastic buckling coefficient k_σ which can be derived from the relationship between out-of-plane deflection (δ) and in-plane loading [43]. Different k_σ values associated with various loading and boundary conditions are illustrated in Figure 6.

| κ_σ: | 0.425 | 1.277 | 4.0 | 5.42 | 4.0 to 23.9 | 23.9 |

Figure 6 Different buckling factors k_σ values associated with various loading and boundary conditions. Adapted from Al-Emrani & Åkesson [43]

For flat web beams, EN1993-1-5 treats flanges as long plates simply supported on three edges (Figure 6), giving a buckling coefficient of k_σ = 0.43. In corrugated web beams, however, boundary conditions differ due to the corrugation parameters. Also, the flange/web thickness ratio has been shown to influence the flange buckling resistance in beams with corrugated webs [44] [15]. EN1993-1-5 considers that the inclined folds provide additional flange support, so the buckling coefficient is defined by Equation (2-3) with an extra $\left(\frac{c_f}{a}\right)^2$ term (with upper limit of 0.6) to account for corrugation. The relationship between the relative slenderness $\bar{\lambda}_p$ and the buckling reduction factor ρ for flanges in trapezoidal corrugated web girders follows the same Winter-curve formula as for flanges in flat web girders. Section 4.4 of EN1993-1-5 [41], Equation (2-4) shown below.

$$k_\sigma = min\left(0.43 + \left(\frac{c_f}{a}\right)^2, 0.6\right) \tag{2-3}$$

$\rho = 1.0 \text{ for } \bar{\lambda}_p \leq 0.748$

$$\rho = \frac{\bar{\lambda}_p - 0.188}{\bar{\lambda}_p^2} \leq 1.0 \text{ for } \bar{\lambda}_p > 0.748 \tag{2-4}$$

Johnson and Cafolla [45] introduced the "enclosing effect" parameter, defined as the ratio of the areas EFGH and ABCD in Figure 3, to capture how corrugation influences flange buckling in corrugated web beams. Based on their experimental findings and finite element analysis, the authors determined that the average flange outstand ($\frac{b_f}{2}$) should be employed in the Eurocode model to calculate the relative slenderness ratio of corrugated web girders for enclosing effect <= 0.14 and a corrugation angle of 30 degrees. For enclosing effect > 0.14, the greater outstand c_f should be used instead.

The German Committee for Structural Engineering's DASt-Richtlinie 015 [34] offers another model for flange buckling that sets an upper limit for the elastic buckling coefficient k_σ at 0.6, which aligns with the provisions specified in EN1993-1-5. Koichi and Masahiro [46] proposed a design relationship with an upper limit of 1.28 for the buckling coefficient k_σ. These models were developed primarily for carbon steel and have been shown to poorly represent flange buckling resistance in beams with corrugated webs [15].

Jäger et al. [15] noted that EN1993-1-5 model often yields unsafe flange buckling predictions for corrugated web girders, mainly because it overlooks the rigidity of the web-to-flange junction. Drawing on both prior research and new experiments, Jäger et al. [15, 31] developed and validated a finite element model specifically for S355 carbon steel girders. Their work involves an imperfection sensitivity analysis to determine appropriate geometric imperfections for FEM-based design, as well as a parametric investigation of the buckling coefficient and the reduction factor. They propose a revised design model for flange buckling which considers the flange-to-web thickness ratio and the enclosing effect. They observed that the specific buckling coefficient for corrugated webs can reduce the buckling curve's plateau length below the 0.748 limit in EN1993-1-5. They also pointed out that Annex C of EN 1993-1-5 recommends an initial out-of-plane deformation amplitude of $\frac{Plate\ Outstand}{50}$ as a general equivalent initial imperfection, though it is not specific to corrugated web beams. Nevertheless, Jäger et al. [15] found that employing $\frac{c_f}{50}$ as the imperfection amplitude, combined with the first eigenmode as the imperfection shape, yields a good estimation of flange buckling resistance in corrugated web beams.

Shear buckling

The research into the shear buckling resistance of corrugated web beams commenced in 1969, leading to numerous studies that identified shear buckling as the predominant cause of failure in girders with corrugated webs subjected to shear. Previous tests have revealed three distinct shear buckling modes: local, global, and interactive buckling [47], as illustrated in Figure 7.
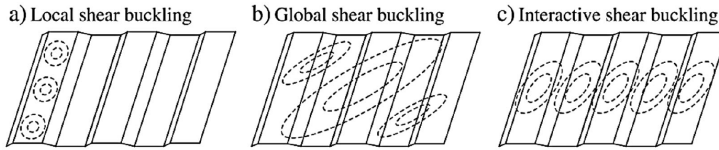

a) Local shear buckling   b) Global shear buckling   c) Interactive shear buckling

Figure 7 Shear buckling modes of trapezoidal corrugated steel webs [47]

The current version of the Eurocode incorporates a design model for estimating the shear capacity of corrugated web beams, detailed in EN1993-1-5, Annex D, Section D.2.2. This model evaluates local and global buckling modes independently, neglecting the interaction buckling mode. Other researchers have focused on establishing the relationship between local and global buckling modes to better predict the shear resistance of corrugated web beams [48] . For example, based on 125 prior tests, Leblouba et al. [48] introduced an equation for shear strength related to the interactive buckling mode (interaction equation of order n = 4).

Regarding the ultimate shear capacity of corrugated web girders, some authors, such as Moon et al. [49] and Sause et al. [50], state that this capacity is dictated by the buckling load. In contrast, Zang et al. [51] argue that flanges can also enhance shear resistance through frame action.

Previous research primarily focused on carbon steel. With reference to stainless steel, the first experimental work was carried out as part of the SUNLIGHT project at Chalmers University of Technology [52] [14]. Four duplex stainless-steel girders (grade EN1.4162), with varying corrugation geometries, were manufactured and subjected to three-point bending tests. When compared to the test results, the EN 1993-1-5 design model yielded relatively conservative strength estimates [53].

Lateral torsional buckling

A beam experiences vertical deflection when subjected to a vertical load. Additionally, if the beam does not possess adequate lateral stiffness or support, it may also deflect laterally in the direction perpendicular to the loading plane, even under lower loads than its capacity in the plane. Lateral deflection and twisting (known as lateral torsional buckling) occur only when the applied moment reaches a critical threshold [54]. Corrugated web girders have been shown to be more resistant to lateral torsional buckling compared to flat web girders [54]. However, for smaller corrugation angles (less than 45deg), Moon et al. [55] found that there is

a minimal difference between flat webs and corrugated webs. The two types have the same pure torsional constant; however, flat webs have a lower warping constant and a larger shear modulus.

For corrugated webs, Annex D in EN1993-1-5 specifies reducing the moment capacity with factor χ for out-of-plane buckling, which should be taken from Section 6.3 in EN1993-1-1. EN1993-1-1 outlines two approaches for analysing lateral torsional buckling for members in bending: the exact method, detailed in Section 6.3.2.2 of EN1993-1-1, and the simplified method using the equivalent compression flange, described in Section 6.3.2.4. The simplified method in EN1993-1-1 is specific to carbon steel; for stainless steel, buckling curve d should be applied, as indicated in Table 5.3 of the Amendment to EN1993-1-4 [56].

Fatigue

Beams with corrugated webs introduce stress concentration points, typically found at the corners of the corrugations. These points exhibit specific fatigue strength properties and are influenced by load effects that differ from those in flat web girders [19, 20, 57]. Several tests on carbon steel corrugated web beams have been conducted and documented in the literature. The experimental results indicated that fatigue cracking often occurs at the junction of inclined and flat folds, identified as the S-point in Figure 8.
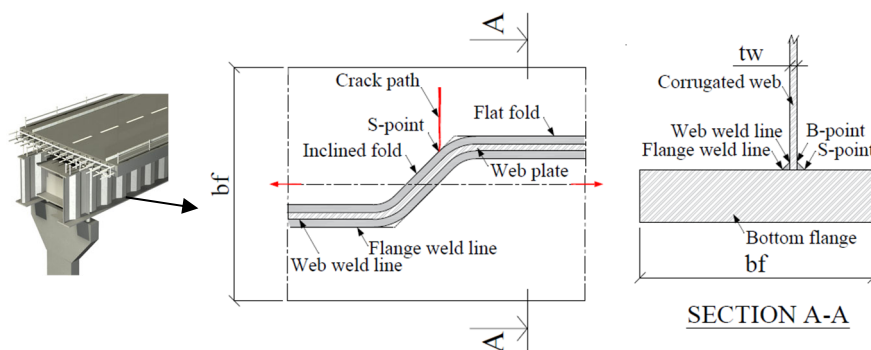
Figure 8 Typical location of fatigue crack in corrugated web girders

Ibrahim et al. [21] [22] tested six hybrid girders under four-point bending, finding cracks in the constant moment zone due to fatigue, with one girder cracking in the middle of the inclined fold due to a weld start-stop point, while all other beams had cracks initiated from an S-point. Sause et al. [23] tested eight large-scale girders with trapezoidal corrugated webs, noting fatigue failures at the S-point in the pure bending area. Kotaki et al. [24] examined two corrugated web specimens, observing fatigue failure in the constant moment zone. Kövesdi & L. Dunai [25] tested six S355 steel beams, with three runouts and three failures at the S-point. Xu et al. [26] studied a prefabricated specimen with oblique flanges to investigate fatigue performance in box girders. The girder failed outside the constant moment zone, with cracks

initiating at the S-point. However, the first observed cracks were in the constant moment region. A girder with a corrugation angle of 45° angle tested by Wang et al. [58] under 3-point bending, developed a fatigue crack at the S-point. Wang et al. [27] also tested 41 corrugated-web T-section members (CWT) with varying corrugation angles. Most specimens failed at the S-point, except one that cracked from a notch in the plate edge. Tong et al. [28] investigated fatigue behaviour using trapezoidal corrugated web T-section members (CWTs). Most fatigue failures occurred at the S-point, though two CWT specimens reached "run-out" after 3 million cycles without crack initiation. In addition to the 18 CWT specimens, one girder tested under four-point bending developed a crack in the pure bending area at the S-point.

A recent study by Zuo et al. [59] experimentally investigated the fatigue behavior of 20 trapezoidal corrugated-web steel girders made of steel grade Q355B. The girders were divided into four groups with varying geometric dimensions and tested under four-point bending. Fatigue failures were observed in three main regions: approximately 70% occurred in the constant bending region, four specimens failed in the combined bending-shear region, and two failed at the concentrated load location. 85% of the girders failed at the S-point in the bottom flange, the remaining specimens exhibited cracks at the web weld toe, referred to as the B-point (Figure 8). Two fatigue failure modes were observed based on crack initiation points. In the first, cracks started at the S-point, propagating through the flange thickness and width, then slightly into the web. In the second, cracks initiated at the weld toe on the web (B-point, Figure 8), penetrating the web and propagating diagonally upward, then following the weld down to the flange and along its thickness and width to the edge.

With reference to duplex stainless steel, several authors, according to Baddoo [60], have examined several types of welded details, and earlier tests demonstrated that the fatigue performance of austenitic and duplex stainless steel is comparable to or slightly greater than that of carbon steel. Accordingly, EN 1993-1-9 recommends using the same S-N curves for stainless steel as for carbon steel. However, EN 1993-1-9 currently does not provide a specific category for the fatigue design of web-to-flange welded details in girders with corrugated webs, irrespective of whether they are constructed from stainless steel or carbon steel.

Residual stresses
Residual stresses in the flanges of corrugated web I-beams arise primarily from two sources: the cooling process near the welds after welding, and the effects of oxygen cutting at the flange tips [61]. The typical distribution of these residual stresses on the flanges of welded shapes is illustrated in Figure 9, which highlights the tension stresses present near the heated areas, while the remainder of the plate experiences compression. In the webs, similar residual stresses occur near the welds and in the bent regions due to cold forming [61].
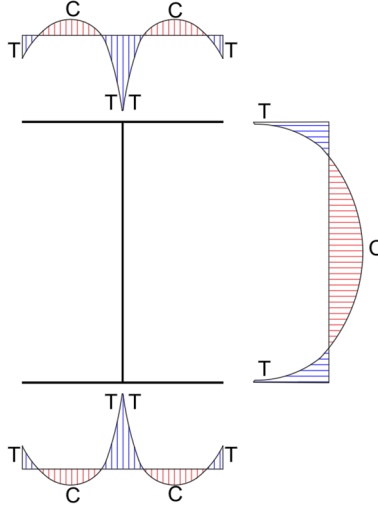
Figure 9 Typical residual stress distribution on flanges in welded shapes. Redrawn from [61]. T: tension, C: compression

In a comparative analysis of residual stress distribution models for flat and corrugated web members, Ning et al.[62] employed the hole-drilling method alongside finite element parametric analysis on S355 corrugated web I-beams. Their findings revealed several key differences in the residual stress distribution models for trapezoidal corrugated web sections. The residual stress distribution in the flanges is asymmetric due to the eccentricity of the trapezoidal corrugated weld shape, leading to continuous changes in residual stresses along the longitudinal direction of the flanges, exhibiting a complexity surpassing that observed in the residual stress of flat web members. The distribution of longitudinal residual stress within the flanges, which corresponds to the inclined web fold, closely resembles that of the flat web members. However, the tensile stress range in the former is approximately 60% greater than that observed in the latter. Tensile residual stress in the flat fold is approximately 10% higher than in the inclined fold. This is attributed to a greater interlock between the flange and the corrugated web. There is minimal residual stress in the middle of the trapezoidal corrugated web due to the accordion effect, where one side of the web is compressed while the other is tensioned. An increase in the corrugation angle results in a corresponding escalation in the range of tensile stress, with an increment of 28% to 31% observed when the angle increased from 30° to 60°. Based on their parametric study, the authors proposed four distinct models to address residual stresses in the flanges. Two of these models are applicable to flat folds (depending on a_3/b_f, see Figure 3), one is for the centre of the inclined fold, and one is intended for the transition area between the flat and inclined folds. In these models, the maximum tensile stress is 0.9Fy above the weld line.

In another experimental study, Lho et al. [61] measured residual stresses at the weld on the bottom surface of the bottom flange of beams

made of steel SM490, finding them to be around $0.4 f_y$. The welding process employed was gas metal arc welding with a continuous $4 \, mm$ fillet weld, performed on one side only.

Residual stresses are known to significantly influence buckling behaviour and load-carrying capacity [31]. For compact flanges, Lho et al. [61] observed that although residual stresses affected the yield point near the welds, the maximum stress in both the top and bottom flanges surpassed $1.0 f_y$. This suggests that the ultimate flexural strength of corrugated web beams with compact flanges can still be based on the flange yield stress. However, in beams with very slender flanges ($c_f/t_f >$ 20), Jager et al. [31] found that the residual stresses had a pronounced impact, reducing bending capacity by approximately 8–9% based on their numerical study on carbon steel S355.

Manufacturers have fabrication tolerances for trapezoidal corrugated web girders, and Annex C in EN1993-1-5 suggests a greater magnitude than the fabrication tolerances for equivalent geometric imperfection. This proposal considers both residual stresses and geometric imperfections, with a suggested value of $\frac{c_f}{50}$ for flange twist. This proposal is not specified for corrugated web girders. Therefore, Jager et al. [31] investigated the applicability of the EN1993-1-5 proposal for flange buckling in corrugated web beams using numerical analysis supported by tests. The author concluded that the EN1993-1-5 suggestion might be applied to flange buckling in carbon steel corrugated web I-beams.

2.2 Duplex stainless steel for bridges

The primary benefit of stainless steel over conventional carbon steel is its capability to resist corrosion [63]. The term "stainless steel" refers to a group of alloys with at least 10.5% chromium that, when exposed to oxygen, create a passive layer of chromium oxide that protects stainless steel from corrosion.

Given their corrosion resistance, duplex stainless steels have recently become more popular in bridge construction, where harsh environmental conditions coincide with high load-carrying demands [3]. These steels offer high strength, ductility, toughness, weldability, fatigue resistance, and durability—all critical for bridges. The grades most suited for bridge applications are 1.4462, 1.4362, and 1.4162 [3].

In Sweden, environmental exposure dictates material selection. According to the document "Requirements for Bridge Construction in Sweden" (Krav Brobyggande) [64], steel components must meet at least corrosivity class C4 unless they are in marine or similarly severe settings. For C4, recommended stainless grades include 1.4162, 1.4362, and the austenitic grades 1.4401, 1.4404, and 1.4571 [64]. Table 1 summarizes these steels' nominal yield strength (f_y,) and ultimate tensile strength (f_u) by thickness. The lean duplex grades (1.4162) are often chosen for their combination of high strength and lower cost (low nickel content) [29].

Table 1 The Swedish Transport Administration's recommendations for stainless steel grades in bridge design

	Grade	$t \leq 8mm$		$t \leq 13.5mm$		$t \leq 75mm$	
		f_y[MPa]	f_u[MPa]	f_y[MPa]	f_u[MPa]	f_y[MPa]	f_u[MPa]
Austenitic	1.4401	240	530	220	530	220	520
	1.4404	240	530	220	530	220	520
	1.4571	240	540	220	540	220	520
Duplex	1.4162	530[e]	700[e]	480[f]	680[f]	450	650
	1.4362	450	650	400	650	400	630

e: $t \leq 6,4$ mm,   f: $t \leq 10$ mm

The use of duplex stainless steel in Europe has increased over the past twenty years. Two examples of road bridges using stainless steel located in Sweden are listed below, with more examples available in [29].

Nynäshamns Bridge-Built in 2011
A composite bridge using EN 1.4162 I-girders (Figure 10a). The municipality chose a composite bridge design that uses stainless steel as the material for the structural I-girders, to avoid the need for maintenance with painting or coating. The bridge is located in Corrosion Resistance Class (CRC) IV, and duplex 1.4162 has performed well under these conditions [29].

Orrhammarvägen Bridge-Built in 2009
Another composite bridge (Figure 10b). It is supported by duplex stainless-steel beams and a bearing plate made of 1.4162 material [29]. The environmental condition is CRC II. The inspection results showed that the performance of 1.4162 was very good [29].

(a) Nynäshamns bridge   (b) Orrhammarvägen Bridge

Figure 10 Examples of composite stainless steel-concrete bridges in Sweden. Photos sourced from [29]

2.3 Genetic algorithms for structural design optimization

The only way to find the optimal solution for a given problem, i.e., the absolute minimum of the objective function would be an "*exhaustive search*", which involves testing all possible values of the design variables. This method is, however, highly time-consuming. To enhance efficiency, optimization algorithms were developed. These algorithms use the results from previous iterations to generate new sets of variables for testing in the current iteration. In essence, these algorithms guide the search towards the areas of the domain that are most likely to contain the optimal solution, drawing on prior experience.

Optimization algorithms can be classified based on their determinacy, as described by Yang [65]. Deterministic algorithms follow a fixed, repeatable path, always yielding the same result for a given input. In contrast, stochastic algorithms introduce randomness into the search process, helping to escape local minima and explore a broader solution space. Stochastic algorithms are further divided into heuristic and metaheuristic methods. Heuristic algorithms rely on trial and error, often finding solutions quickly but without guaranteeing optimality. Metaheuristic algorithms blend randomization with local search, improving solution quality while reducing the risk of getting stuck in local optima. As Yang [65] notes, this balance between global and local search increases the likelihood of finding a better global solution.

Genetic algorithms, as defined by Yang [65], are population-based metaheuristic algorithms. Yang discusses their applicability to both continuous and discrete optimization problems through appropriate encoding methods, which make them suitable for structural engineering design tasks. Several studies have explored their use in optimizing various civil engineering structures and materials [66]. More recently, the bridge industry has shown increased interest in structural optimization, aiming to enhance design aspects such as environmental impact and cost by focusing on material selection, design variables, and structural configurations [66] [67].

Mapping the genetic algorithm to natural selection
The Genetic Algorithm (GA) is inspired by Darwin's theory of natural selection, where the fittest individuals are more likely to survive and reproduce in the face of environmental pressures and threats [68]. Members who are the fittest have a higher chance of surviving than others. They are more likely to adapt to changing environments, and their children may acquire and learn their qualities, generating even more fit future generations. Furthermore, genetic mutations occur at random in members of a species, and some of these variations may boost the probability of the long-term survival of fit individuals as well as their evolutionary descendants. Each individual created by the GA (called a chromosome) represents a potential solution to the optimization problem

at hand. Each chromosome contains genes that reflect decision variables. Individuals' fitness values determine their ability to survive. Genetic operators such as crossover and mutation produce children, which represent new solutions. Parents are picked in such a way that their likelihood of selection is proportional to their fitness scores. The greater the fitness value, the greater the chances of survival and reproduction [68].

According to Bozorg [68], standard GA starts with a population of randomly generated potential solutions (individuals). The fitness of the individuals is calculated, and some of them are chosen as parents based on their fitness levels. By applying the crossover operator to the parent population and subsequently the mutation operator to their offspring, a new population (or generation) of possible solutions (the children's population) is created. Iterations in which the original generation (an old individual) is replaced by a new generation (children) are repeated until the stopping requirements are met. The number of children belonging to the three categories (elite, mutation children, and crossover children) is defined by the user. Elite and crossover children represent the local component of the search, while mutation children represent the global component obtained through randomization.

Genetic algorithm Python library "geneticalgorithm"
"geneticalgorithm" is a Python library distributed on "https://pypi.org/" for implementing standard and elitist genetic algorithms (GA). The algorithm was developed by Solgi [69], and it provides an easy implementation of the genetic algorithm (GA) in Python. It can be installed for free using the package manager "pip".

For design optimization of structural elements, it is necessary to limit the utilization ratios to values lower than one. Solgi [69] suggests addressing a penalty function that is larger than the maximum value of the objective function for such optimization problems with constraints if this value is known or can be estimated. As a result, if a trial solution, despite having a small objective function, is outside of the feasible zone, the penalized objective function (fitness function) is poorer than any possible solution. However, in cases where the optimum is precisely on the edge of the viable zone (or extremely close to the constraints), which is common in some types of problems, a highly rigid and significant penalty may prevent the algorithm from approaching the optimal region. In this case, a proper penalty function is needed [69]. More information about the definition of the penalty function can be found in Bozorg's book [68]. Bozorg [68] and Solgi [69] also provide definitions for the genetic algorithm parameters, which are listed below:

- Initial population size, which determines how many trial solutions there will be in each iteration. The population may be seen as an M x N matrix, where M is the total number of solutions for each variable and N is the total number of design variables (genes) that will be optimized.

- Parents portion: the percentage of the population that is made up of individuals from the preceding generation.
- Mutation probability: determines the probability that a random value will be substituted for each gene in each solution. The default setting set by Solgi is 0.1, or 10%.
- Elite ratio: identifies the elite percentage of the population. One percent, or 0.01, is the default setting set by Solgi. For instance, if the population is 100 and the elit_ratio is 0.01, there is only one elite in the population. If this parameter is set to zero, "geneticalgorithm" will utilize a standard genetic algorithm rather than an elitist GA.
- Crossover probability: controls the probability that an existing solution will pass on its genome to subsequent trial solutions; the default value set by Solgi is 0.5 (or 50%).
- Crossover type: there are three options to choose from: one-point, two-point, and uniform crossover functions. The difference between these types is explained in Bozorg et al.'s book [68]. Uniform crossover is the default set by Solgi.
- The maximum number of iterations without improvement: The genetic algorithm stops and reports the best-identified solution before the maximum number of iterations is reached if the objective function is not improved throughout the number of subsequent iterations defined by this parameter. None is the default value.

2.4 Life cycle assessment (LCA)

LCA, according to the international standard ISO 14040:2006 [70], is a method to assess the environmental impacts of a product's life cycle, from material extraction to manufacture, use, and disposal. The analysis is an iterative process divided into four phases:

1. Goal and Scope Definition: This stage establishes the purpose and boundaries of the LCA, ensuring the assessment is focused and aligned with the intended objectives, such as comparing products or improving processes.
2. Life Cycle Inventory (LCI): Here, data on inputs (like raw materials and energy) and outputs (such as emissions and waste) are collected, providing the necessary information to evaluate environmental impacts.
3. Life Cycle Impact Assessment (LCIA): This stage analyzes the LCI data to assess potential environmental impacts, translating raw data into meaningful indicators like global warming potential (GWP) and resource depletion.
4. Interpretation: The final stage involves drawing conclusions from the LCA results, guiding decision-making for product improvement, sustainability strategies, or stakeholder communication.

The European Standard EN 15978:2011 provides a systematic approach for evaluating a building's environmental performance based

on Life Cycle Assessment (LCA). All phases of the building life cycle are covered by the assessment approach. The life cycle stages and modules of a building, according to European Standard EN 15978:2011, are shown in Table 2.

There are various impact assessment methods to evaluate the potential environmental impacts using different indicators, e.g., global warming potential or acidification potential. Contemporary building-related Life Cycle Assessments (LCAs) primarily focus on quantifying greenhouse gas emissions [71]. The LCIA data needed for the impact assessment of a construction project usually comes from generic databases such as Ecoinvent or from product-specific Environmental Product Declarations (EPD), which follow EN 15804 [72].

Table 2 Life cycles modules for building construction (adapted from EN 15978:2011) [73]

Product stage			Construction stage		Use stage							End of Life stage				Benefits and loads beyond the system boundaries
A1: Raw material supply	A2: Transport	A3: Manufacturing	A4: Transport	A5: Construction/ installation	B1: Use	B2: Maintenance	B3: Repair	B4: Replacement	B5: Refurbishment			C1: Deconstruction- demolition	C2: Transport	C3: Waste processing	C4: Disposal	D: Reuse, recovery, and recycling potential
									B6 Operational energy use							
									B7 Operation water use							

2.5 Life cycle cost analysis (LCCA)

Life cycle cost analysis (LCCA) is a method for evaluating the life cycle cost over a given assessment time [74]. Many bridge management systems employ LCCA as a fundamental tool for determining the best strategy based on the remaining life span [74].

LCCA is a helpful method for determining whether bridges are cost-effective since it considers all expenditures, from acquisition through destruction [75]. The LCCA for a bridge should include the initial expenditures, material expenses, and expected maintenance costs during the bridge life cycle [76]. Moreover, the user costs associated with traffic delays, when the average daily traffic volume is high, influence the bridge's total life cycle costs and need to be considered [6, 77].

As the costs considered in LCCA occur at different points in time, it is necessary to adjust them to a common point in time for meaningful comparison. Several methods are available for conducting LCCA, including the Equivalent Annual Cost (EAC) method and the Net Present Value (NPV) method [76]. Among these, the NPV method is the most widely used for comparing past, present, and future cash flows with those of today [76] [78]. To account for the time value of money, a discount rate is applied, enabling all expenditures to be expressed in terms of their present value. The NPV can be calculated using Equation (2-5).

$$NPV = C.\left(\frac{1+i}{1+d}\right)^n \hspace{3cm} (2\text{-}5)$$

Where C represents the current cost, i is the escalation rate, d is the discount rate, n is the year in which the cost occurs within the study period.

Chapter 3

3 Conducted studies and results

3.1 Overview

The work in this thesis is built on five studies. Study **A** compares the duplex corrugated-web I-girder with the traditional S355 flat-web girder and, in a later complementary analysis, with S460. Study **B** explores the flange buckling problem in duplex corrugated web I-girders through a numerical parametric analysis. Study **C** examines the relevant load effects for fatigue design of the flange-to-web welded detail using both experimental and numerical methods. Using published experimental data, Study **D** conducts a fatigue assessment of the flange-to-web welded detail in carbon steel corrugated web members. Lastly, Study **E** involves an experimental program to evaluate the fatigue resistance of the same detail in duplex EN1.4162 steel. The results of these studies are documented in the appended papers (Papers I-VI). An overview of the current work and the main findings is depicted in Figure 11.
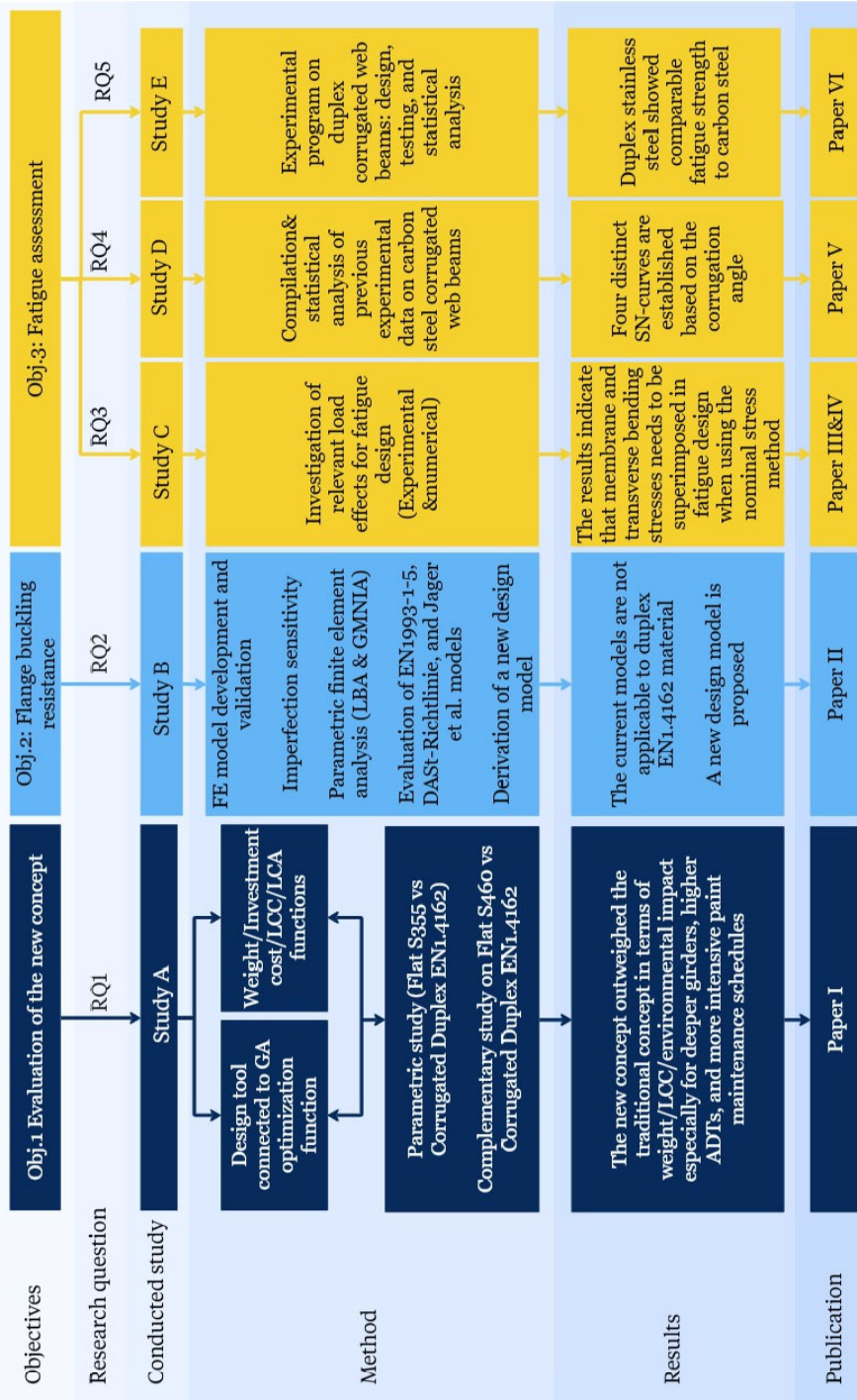
Figure 11 Overview of research work

3.2 Study A: Concept evaluation

This study aims to explore the benefits of using stainless steel corrugated web I-girders as an alternative to carbon steel flat web I-girders in composite road bridges and to investigate if this design solution can reduce initial investment costs, bridging the cost gap between carbon and stainless steel, thereby making the long-term benefits of stainless steel more attainable. This chapter provides a summary of the work, with further details available in **Paper I**.

3.2.1 Description of the study

A design optimization tool based on a genetic algorithm is developed for the design of steel-concrete composite bridges. The tool offers flexibility by optimizing bridges with either flat or corrugated webs. The objective of the optimization can be set to minimize either the total weight, investment cost, life cycle cost (LCC), or environmental life cycle impact (LCA), while satisfying the structural requirements, keeping utilization ratios below 1. The optimization is implemented in Python using the "geneticalgorithm2" module developed by Demetri Pascal [79]. A schematic representation of the optimization routine is shown in Figure 12.
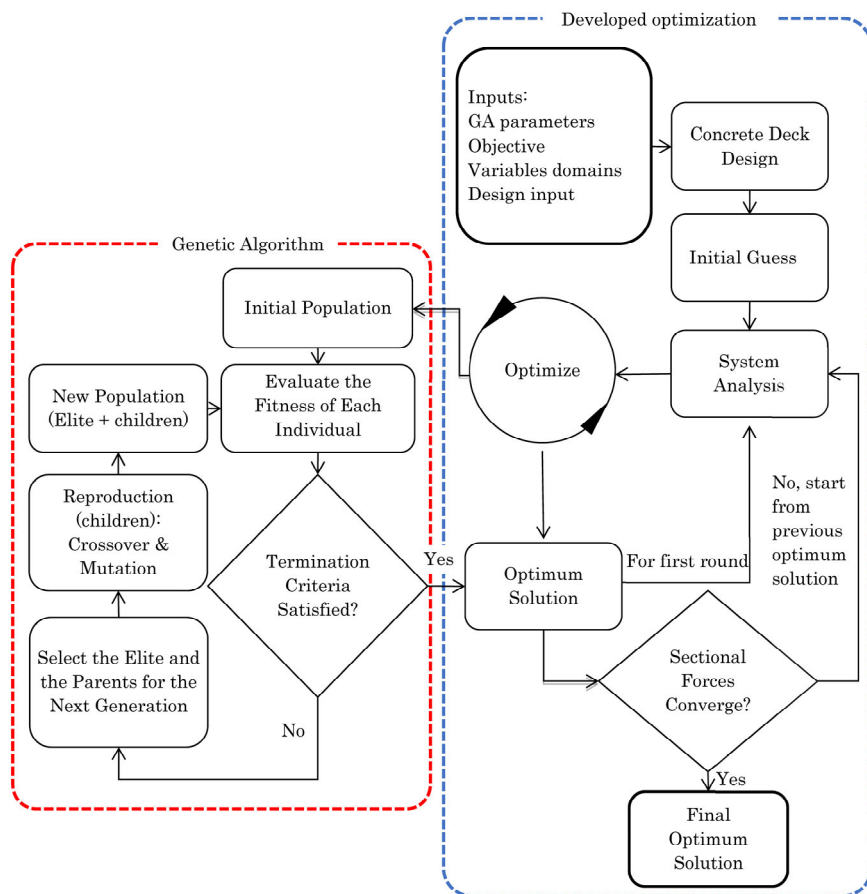
Figure 12 A schematic representation of the developed optimization tool

The optimization process in Figure 12 can be explained through the following key steps:

- **Inputs**: The optimization process starts with essential inputs, which include genetic algorithm parameters, specific optimization objective, design variables domains (ranges of potential values), additional design inputs such as materials grades, bridge span lengths and widths, environmental inputs, and a cost/environmental impact database for LCC and LCA, as well as the inflation and discount rates.
- **Concrete Deck Design**: The concrete deck is designed with typical thicknesses ranging from 250 to 350 mm [80]. As such, it's not subject to optimization.
- **Initial Guess & System Analysis:** The bridge is segmented into seven possible sections per span to determine the optimal values for various geometrical parameters, including the bridge girder dimensions, web corrugation parameters, and the spacing

between cross beams. The process starts with an initial guess of these design variables, derived from their respective domains. This estimation is then employed to perform an initial system analysis that calculates the sectional forces along the bridge.

- **Optimize**: In this phase, multiple solutions are generated based on the defined variable domains. A structural evaluation is then performed on these solutions according to Eurocode standards [81] [82] [83] [84] [85] [41] and relevant Swedish national regulations [86] [64]. During this phase, utilization ratios are calculated, and constraints are assessed. If any ratios exceed acceptable limits, penalties are applied to promote adjustment. The design variables are then updated to minimize the fitness function, resulting in a set of optimal design variables based on the initial analysis (referred to as the "*Optimum Solution*" in Figure 12.

- **Re-Optimization Cycle**: the system analysis is then updated with the optimal design variables ("Optimal Solution"), and the optimization cycle continues iteratively until the convergence criteria are met, at which point the design is considered optimal (referred to as *"Final Optimum Solution"* in Figure 12).

Figure 13 provides a summary of the design variables subjected to optimization, as well as the fixed geometrical parameters.
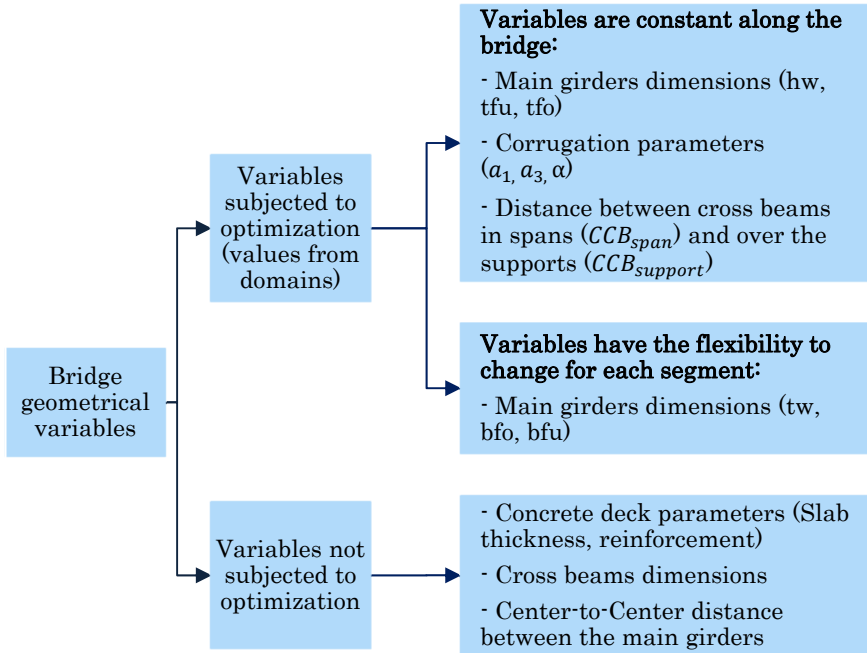

Figure 13 Illustration of the bridge parameters that undergo optimization and those that do not

Additionally, calculation models (functions) have been developed to calculate the total weight, investment cost, life cycle cost (LCC), and life cycle environmental impact. The life cycle stages of a building, as defined by the European Standard EN 15978:2011 and summarized in Table 2, are adopted as a general framework for conducting both the Life Cycle Assessment (LCA) and Life Cycle Cost Analysis (LCCA) for bridges. The total environmental impact is calculated by aggregating the contributions from various life cycle stages, including manufacturing, construction, usage, and end-of-life. CML 2001 methodology is applied for the environmental impact assessment with a focus on Global Warming Potential (GWP) environmental indicator, expressed in kilograms of CO_2-equivalent. With reference to LCC, the Net Present Value (NPV) method, discussed in Section 2.5, is employed.

System boundaries and schematic representations of the assessment frameworks are shown in Figure 14 for LCA and Figure 15 for LCCA. Detailed calculation models are provided in Figure 35, Table 13, Figure 36, and Table 14 in the Appendix, with further information available in references [87] and [88]. These models were originally developed by SYU [89] and subsequently refined by Nissan et al. [87], in collaboration with sustainable design experts from the Division of Building Technology at Chalmers.
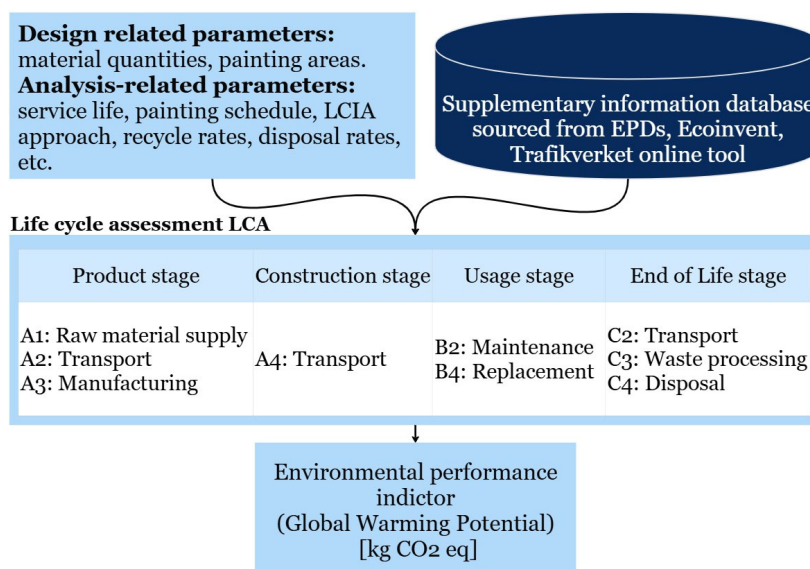
Figure 14 The framework of the conducted LCA
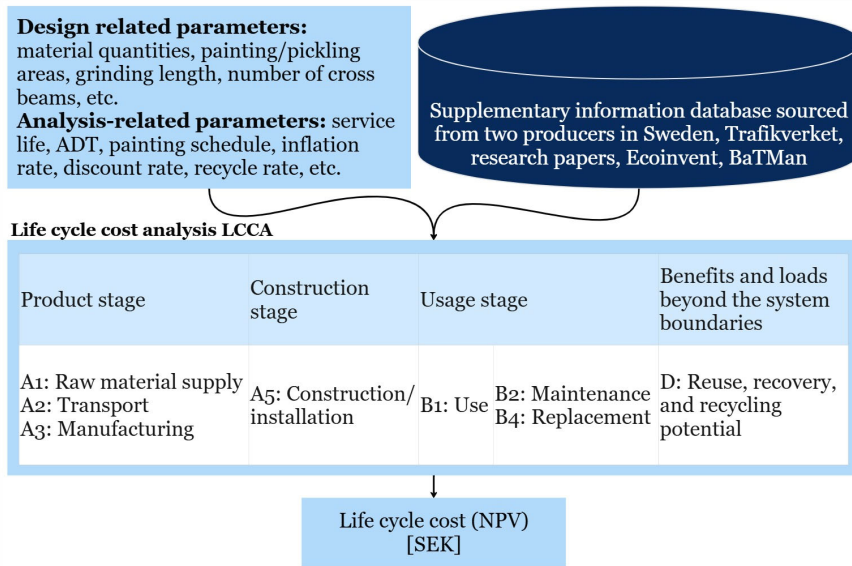
Figure 15 The framework of the conducted LCCA

The developed tool is used to perform multiple parametric studies on a reference bridge, specifically a one-span steel-concrete composite bridge with twin flat-web carbon steel I-girders of span 52 meters located in Sweden. The study compares stainless-steel corrugated web I-girders with traditional carbon steel flat web I-girders under various design parameters. The research begins by examining the impact of the chosen optimization objective, followed by analyses of the effects of painting schedules, average daily traffic (ADT), possible girder height restrictions, and bridge span length. The designations for the full parametric study are presented in Table 4 in **Paper I.**

3.2.2 Summary of results

The detailed results of the parametric study are presented in Table 15 to Table 20 in the Appendix and are summarized below.

Optimization Objective
Table 3 and Table 4 present the optimization outcomes for various objectives for the reference bridge with the two examined concepts.

For the carbon steel, Table 3 shows that the optimization results are significantly affected by the chosen objective, whether it is weight, investment cost, life cycle cost (LCC), or life cycle environmental impact. When the optimization objective is set to minimize costs (either investment or LCC), the algorithm prioritizes the reduction of the painting area as painting costs are considerable—20–29% of the initial investment and 36–55% of the total LCC in the studied cases— even if this results in heavier design solutions. In contrast, if the optimization

objective is set to minimize life cycle impact, the algorithm prioritizes weight reduction because material production is the primary environmental burden.

For stainless steel, Table 4 shows that the quantity of material used is the key factor influencing both cost and life cycle impact, and the optimization consistently seeks to minimize material usage, regardless of the objective function.

Table 3 Optimal design solutions for different optimization targets for flat web carbon steel (S355) concept (ID1- ID5 in Paper I)

Objective	Painting area [m^2]	Weight [ton]	LCC [$MSEK$]
LCC	830	84	4.324
Weight	1000	75.4	4.538
LCA	973	76	4.539
Investment cost	916	80	4.427

Table 4 Optimal design solutions for different optimization targets for corrugated web stainless steel (EN1.4162) concept (ID5- ID8 in Paper I)

Objective	Pickling area [m^2]	Weight [ton]	LCC [$MSEK$]
LCC	970	57	3.296
Weight	999	56	3.279
LCA	945	59	3.463
Investment cost	969	57	3.331

Investment Costs

The results indicate that using corrugated web stainless steel I-girders can substantially reduce the initial investment cost gap between carbon and stainless steel. Despite stainless steel being three times more expensive than carbon steel, the investment cost for stainless steel concepts was only 1–11% higher in most of the studied cases, owing mainly to weight savings (ranging between 20–38%) and eliminating the need for painting.

Table 5 shows one example where the investment cost for the stainless-steel option was only 4% higher than the traditional concept. The corrugated web design allowed for thinner webs and smaller flanges with deeper girder, resulting in material savings of 32%. Additionally, the elimination of painting and grinding during production, along with reduced cutting and welding costs due to thinner plates and less material usage, as illustrated in Figure 16, further contributed to the lower production costs associated with stainless steel corrugated web girders.

Table 5 Costs and footprint comparison for ID1 and ID5 in Paper I

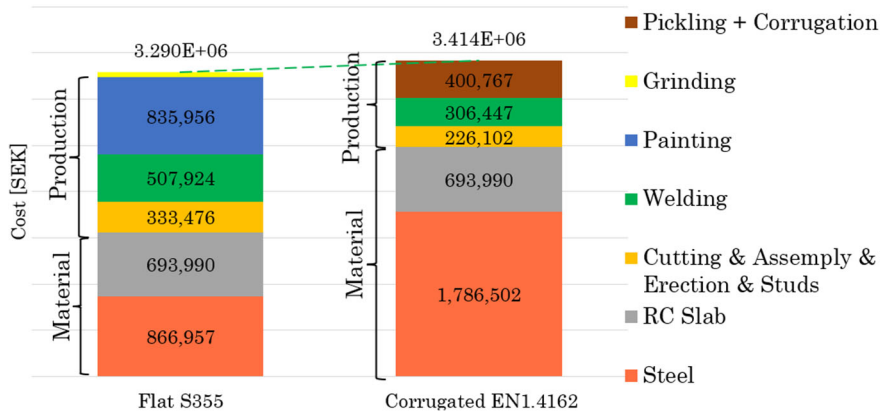|	Flat S355 (ID1)	Corrugated EN1.4162 (ID5)	Saving
Total weight [ton]	84	57	-32%
Flanges weight [kg]	52 308	39 125	-25%
Web weight [kg]	26 171	13 321	-49%
Production cost [SEK]	1 731 959	936 996	-46%
Investment cost [SEK]	3 290 301	3 413 809	+4%
Maintenance Cost [SEK]	1 060 821	0	-100%
LCC [SEK]	4 324 213	3 296 227	-24%
LCA [kg CO$_{2eq}$]	338 502	211 991	-37%

Figure 16 Breakdown of investment costs for ID1 and ID5 in Paper I

Life Cycle Costs (LCC)

The results showed that the adopted paint maintenance schedule significantly affects the LCC outcomes. Two distinct paint maintenance schedules were compared: one obtained from Trafikverket (Table 5 in Paper I), and one—more intensive— sourced from the literature (Table 6 in Paper I), with the comparison presented in Table 6.

Notably, even under the more conservative schedule, the stainless-steel corrugated web concept achieved an LCC saving of 24% compared to traditional carbon steel flat web girders, increasing to 43% with the more intensive schedule. These additional savings are primarily due to the absence of painting during maintenance for stainless-steel designs. Across the studied cases with a height limitation of 3 m, the LCC savings ranged from 20% to 49% compared to the traditional flat web design.

Table 6 Comparison of three optimized solutions of girders ID1, ID9, and ID5 in Paper I

	Weight [ton]	LCC [MSEK]	Footprint [Kg CO2eq]
Flat S355-TRV schedule	84	4.3	339k
Flat S355-Rossi et al. schedule	93	5.8	368k
Corrugated EN1.4162	57	3.3	212k
Saving			
Flat S355-TRV schedule vs Corrugated EN1.4162	-32%	-24%	-37%
Flat S355-Rossi et al. schedule vs Corrugated EN1.4162	-39%	-43%	-42%

Inflation and Discount Rates

The assumed discount and inflation rates are two parameters that might have a considerable impact on LCC results. In economics, the inflation rate indicates the different growth of certain products and/or service costs over time. It is used to indicate price fluctuations (of building materials, energy costs, or labour) that deviate from the overall inflation rate [90]. The discount rate is defined as 'the component indicating the time value of money that is used to transform cash flows happening at different times to a common time'. Discounting implies that future costs are less important than current costs. Future expenses are just as important as present costs when $d = 0\%$. The higher the discount rate, the greater the significance placed on the near-present and the less importance given to what happens in the future [90]. In theory, employing a high discount rate will favour alternatives with low investment costs and high usage costs, and vice versa. Sensitivity analysis of the influence of changing the discount rate on the final choice is critical in both bridge management and investment because it allows decision-makers to assess their confidence in selecting the best option [91].

The results presented in previous sections are based on predictions of a 1.5% inflation rate and a 3.5% discount rate. These values were obtained from Safi [91] and based on notations from Trafikverket 2013. To explore the effects of changes in discount and inflation rates on the conclusions, a sensitivity analysis was conducted. In addition to the baseline discount rate of 3.5%, two alternative rates, 2% and 5%, were examined. Similarly, alongside the inflation rate of 1.5%, two additional rates of 0% and 3% were tested.

Despite the uncertainties posed by inflation and discount rates in life cycle cost analysis, all examined scenarios in the study yielded LCC savings when employing the stainless-steel corrugated web concept (Section 6.3 in Paper I).

Average Daily Traffic (ADT) and Heavy Vehicles (N_{obs})
A bridge's average daily traffic (ADT) is determined by its location and whether it is in an urban or rural region with varied traffic flow rates. The volume of ADT is proportional to the number of heavy vehicles indicated in each slow lane, designated as N_{obs} [92], which influences the fatigue design of the bridge structure [83]. The influence of ADT and N_{obs} can significantly impact the optimal design. A higher volume of heavy vehicles may reduce the benefits of utilizing higher-strength stainless steel, as fatigue becomes more governing. Conversely, an increase in ADT tends to elevate user costs, thereby making stainless steel a more economically feasible option. This study examined three scenarios involving various combinations of ADT and N_{obs}. The stainless-steel corrugated web concept consistently showed strong potential for LCC savings of 43-49% across the three combinations analysed (Section 6.4 in Paper I).

Height Limitations
The available free height beneath the bridge often restricts the permissible web height in bridge design. Additionally, one of the primary challenges of using deep girders for flat web designs is the risk of web buckling as the web height increases. This necessitates the incorporation of longitudinal or/and transverse stiffeners or a thicker web, both of which lead to higher material consumption. However, due to the high shear buckling strength of corrugated web plates, they present less of an obstruction, making deeper girders a more viable option.

The study evaluated the influence of maximum girder height on LCC savings. Reducing the height limit from 3 m to 1.5 m decreased the LCC saving from 20% to 5% and increased the investment cost gap from 11% to 26%, indicating that the concept is more advantageous for deeper girders.

Span Length
In the final step of the parametric investigation, the objective was to assess the relevance of the conclusions drawn for different span lengths. The optimization process is carried out for two span lengths at three distinct levels of ADT: low, medium, and high, corresponding to N_{obs} values of 50,000, 125,000, and 500,000.

The results indicated that the potential for weight and LCC savings with stainless steel corrugated web girders is comparable for both short (30 m) and long (52 m) span lengths across various ADT and N_{obs} combinations —ranging from 20–26% for long-span bridge cases and 18–22% for short-span cases— indicating that these benefits can be achieved across a wide range of span lengths (Section 6.6 in Paper I).

LCA results
The environmental impact, expressed as Global Warming Potential (GWP), was 32–42% lower than that of the traditional concept across the studied cases. Material production was found to be the dominant

contributor to the overall environmental burden (Fig. 6 in Paper I). Stainless steel offered a clear advantage in this regard, with a unit GWP of 1.7 kg CO_2 eq/kg compared to 2.63 kg CO_2 eq/kg for S355 carbon steel. This lower emission factor, combined with the weight savings achieved by the corrugated web design, led to a notable reduction in total GWP. It should be noted, however, that these results depend on the Environmental Product Declarations (EPDs) provided by the steel manufacturer, and variations in data sources influence the calculated benefits.

3.2.3 Complementary study-comparison with S460

A complementary study involving carbon steel grade S460 is conducted to gain further insight into how the results would vary for a higher grade of carbon steel with a yield strength closer to duplex EN1.4162. The price of S460 is assumed to be 1.13 times the cost of S355. The optimization is performed on three design alternatives: Flat S355, Flat S460, and Corrugated EN1.4162, across two scenarios of ADT and N_{obs}. This approach allowed for consideration of cases where fatigue limit state (FLS) governed the design as well as when Ultimate Limit State (ULS) governed.

The results, presented in Figure 17, illustrate that for low ADT, the design is governed by ULS with a relatively low FLS utilization ratio. In this case, the S460 solution achieved a slightly lower life cycle cost compared to the S355 option. This reduction is attributed to weight savings from the higher-strength steel, although these were partially offset by higher material costs. At high ADT levels, where fatigue combined with ULS governs the design, S355 and S460 exhibited close life cycle costs. In this case, the benefits of weight reduction were smaller, and user costs increased for both carbon steel options. Notably, EN 1.4162 corrugated girders outperformed both flat S355 and S460 alternatives under both traffic scenarios.

Worth mentioning here that Rossi et al. [8] similarly concluded that if the initial cost of high-strength S460 steel does not exceed 1.13 times that of mild S355 steel, their total lifecycle costs are the same.
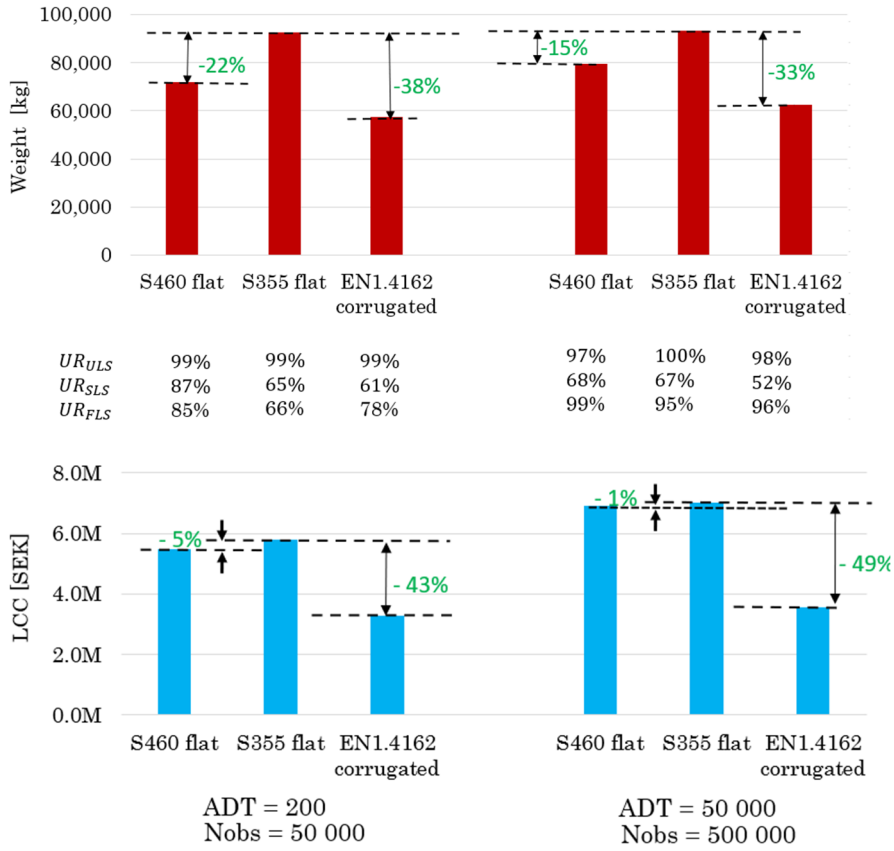
Figure 17 *Comparison of life cycle cost and weight for three girder design alternatives: flat S355, flat S460, and corrugated EN 1.4162. The painting schedule is sourced from Rossi et al.[93]*

3.3 Study B: Flange buckling

Following the evaluation of the stainless-steel corrugated web concept, this thesis focuses on two main design aspects: the flange buckling problem and the fatigue assessment. This section presents the conducted study related to flange buckling, while the next section covers the fatigue assessment.

The study on flange buckling involved a numerical analysis of the buckling behaviour of duplex stainless-steel I-girders with corrugated webs subjected to pure bending. This research fills the gap in existing studies on flange buckling in such beams, particularly as current design standards like EN1993-1-5 are based on carbon steel and may underestimate the buckling resistance of duplex stainless-steel I-girders. Based on the findings, a new buckling curve and design model are proposed to calculate the flange buckling resistance of these girders. This chapter provides a summary of the work, with additional details available in **Paper II**.

3.3.1 Description of the study

To establish a design procedure similar to that adopted in EN1993-1-5 for flat web girders, the method illustrated in Figure 18 is employed in this work for corrugated web girders. The study employs finite element analysis (FEA), specifically GMNIA analysis. A parametric finite element model is developed and validated through experiments conducted by Jager et al. [15, 31, 94] and Elamary et al. [36] on carbon steel beams. Subsequently, the material model is updated to reflect duplex stainless steel 1.4162, in accordance with EN1993-1-4.
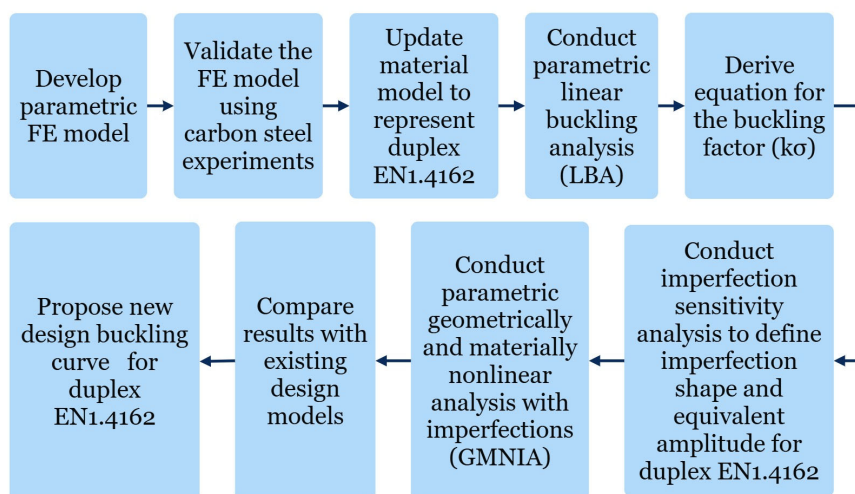
Figure 18 An illustration of the procedure that is used to address the flange buckling problem

The developed finite element parametric model is then employed to analyse 410 girders with dimensions typical for bridge girders. The chosen parameters are summarized in Table 7, which outlines the investigated range for various parameters.

Table 7 Investigated parameters ranges. The notations are provided in Figure 3

Parameter	Investigated range
$\alpha \ [deg]$	$30 - 45 - 60$
b_f/a_3	$2 - 2.4 - 2.7 - 3 - 3.2 - 3.3 - 4 - 5 - 6 - 6.7 - 8$
a_1/a_3	$2 - 3 - 4$
t_f/t_w	$2.5 - 3.5 - 4.17 - 5 - 5.83 - 6.25 - 8.33 - 8.75 - 12.5$
$b_f \ [mm]$	$400 - 600 - 800 - 1000$

Initially, a linear buckling analysis (LBA) is conducted on the 410 girders to estimate the buckling stress and the corresponding buckling factor, denoted as k_σ. The k_σ factors obtained are compared to the established equations in EN1993-1-5 [41] and Jager et al. [15]. After that, a new equation for the buckling factor k_σ is derived using regression analysis and a genetic algorithm procedure to find the best fit. This analysis considers parameters believed to influence the buckling factor, including the corrugation depth to flange width ratio $(\frac{a_3}{b_f})$, the web-to-flange thickness ratio $(\frac{t_w}{t_f})$, the flange width to flange thickness ratio $(\frac{b_f}{t_f})$, and the folded to unfolded lengths of one-half wave ratio $(\frac{w}{s})$. The notations are referenced in Figure 3.

The resulting buckling modes are then used as initial imperfection shapes, with an equivalent amplitude of $c_f/50$, in subsequent geometrically and materially nonlinear analysis with imperfections (GMNIA). The imperfection amplitude is defined based on an imperfection sensitivity study conducted on the same test data used for model validation, justifying the use of an initial imperfection magnitude of $c_f/50$ (where c_f represents the larger flange outstand) in conjunction with the first eigen buckling mode for duplex stainless steel. A comparison of two specimens is illustrated in Figure 19.
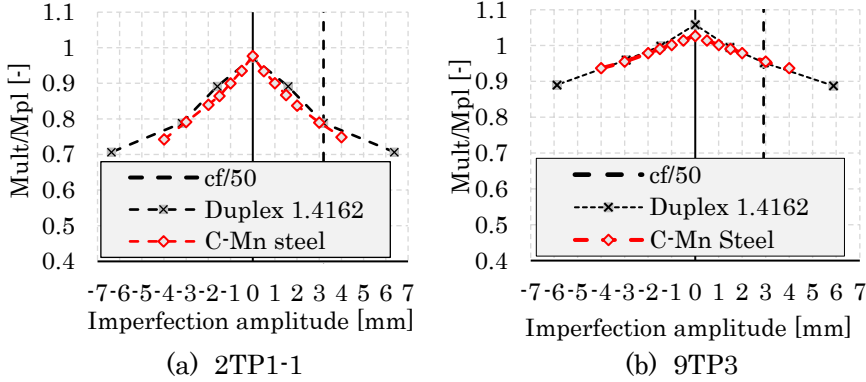
(a) 2TP1-1   (b) 9TP3

Figure 19 Imperfection sensitivity curves for specimen 9TP3 and 2TP1-1 for Carbon steel and EN1.4162

The GMNIA analysis aims to determine the ultimate moment capacity of each girder. The moment capacities are then compared to those estimated using previously established design models. Based on these results, a new buckling curve is derived.

3.3.2 Summary of results

The results from the FEA are compared to earlier models for C–Mn steel, including the EN1993–1-5 [41] model, the model developed by Jáger et al. [15], and the DASt-Richtlinie 015 [34] model. It is found that these models are not applicable to duplex EN1.4162. Consequently, this study introduced new design equations for both the buckling factor and the reduction factor. The analysis of linear regression and the genetic algorithm on linear buckling led to an equation for the buckling factor, κ_σ, shown in Equation (3-2). The findings from the geometric and material nonlinear analysis led to a proposed buckling curve specifically for duplex stainless steel corrugated web girders, shown in Figure 20 and defined by Equation (3-4). Additionally, the limit of CSC4 is found to be $\bar{\lambda}_p > 0.4$, which corresponds to $c_f/t_f/\varepsilon/\sqrt{k_\sigma} < 11.36$.
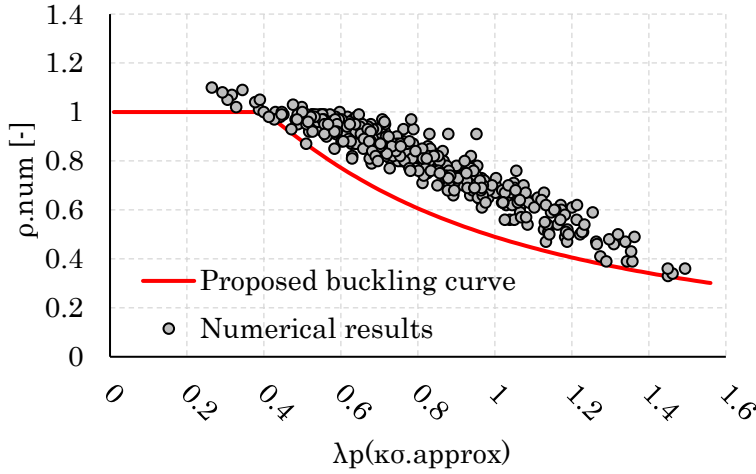
Figure 20 The developed buckling curve for flanges in duplex girders with corrugated webs

Based on these findings, a design procedure to account for flange buckling in duplex stainless-steel corrugated web beams is proposed as follows: Define the limit for cross-section class 4 as follows:

$$if\ c_f/t_f > 11.36\varepsilon\sqrt{\kappa_{\sigma.corr}} \rightarrow \text{the flange is in CSC4} \tag{3-1}$$

Where the buckling coefficient is defined as:

$$\kappa_{\sigma.corr} = 1.7 - \sqrt{\frac{a_3}{b_f}} + 0.76 \cdot \frac{t_w}{t_f} + 0.94\left(\frac{b_f}{t_f}\right)^{0.17} - 2.56\left(\frac{w}{s}\right)^2 \tag{3-2}$$

When the flange is in CSC4, calculate the flange's relative slenderness as follows:

$$\bar{\lambda}_p = \sqrt{\frac{f_y}{\sigma_{cr}}} = \frac{c_f/tf}{28.4\varepsilon\sqrt{\kappa_{\sigma.corr}}} \tag{3-3}$$

Determine the buckling reduction factor from the following equation:

$$\begin{aligned}
\rho_{corr} &= 1.0 && \text{for} && \bar{\lambda}_p \leq 0.4 \\
\rho_{corr} &= \frac{0.69}{\bar{\lambda}_p} - \frac{0.1}{\bar{\lambda}_p^{\ 2}} - 0.1 \leq 1.0 && \text{for} && \bar{\lambda}_p > 0.4
\end{aligned} \tag{3-4}$$

The moment capacity for flange buckling can now be obtained from:

$$M_{ult.\ Corr} = \rho_{corr} \cdot b_f \cdot t_f \cdot (h_w + t_f) \cdot f_{yf} \tag{3-5}$$

3.4 Study C, D, and E: Fatigue assessment

This section presents the study conducted to address the second design aspect (Obj.3): fatigue assessment of the flange-to-web welded detail in corrugated web I-girders. To conduct a fatigue assessment on a specific detail, it is essential to identify the relevant load effects and select the appropriate S-N curves (i.e., detail categories) for the fatigue analysis.

As previously discussed, the crack in the examined detail typically occurs at the corners of the corrugation, referred to as the S-point (Figure 8) and propagates through the thickness and width of the flange plate. This study begins with Study **C**, which includes an investigation into the stress distribution in the beam flanges through finite element analysis (FEA) and experiment, aiming to comprehend the variations in stress due to bending and shear at potential crack initiation points, and to check whether these load effects can be superimposed for fatigue design.

Furthermore, in Study **D**, a comprehensive review of 86 fatigue tests on carbon steel girders from existing literature is carried out, with results categorized based on the corrugation angle and evaluated using statistical analysis. Four distinct detail categories based on the corrugation angle are proposed for carbon steel.

Finally, in Study **E**, an experimental program involving 15 duplex EN1.4162 beams was conducted to evaluate the fatigue performance of the same detail in duplex stainless steel. The results are evaluated using statistical analysis and compared with the established detail categories for carbon steel in the previous study.

This chapter provides a summary of the work, with further details on the load effects in **Papers III and IV**, the evaluation of previous tests in **Paper V**, and the experimental work in **Paper VI.**

3.4.1 Study C: Relevant load effects for fatigue design

To understand the various load effects that influence the stress distribution in the flanges of corrugated web girders and their potential impact on crack initiation points, finite element models are developed using Abaqus CAE 2020 to model simply supported beams subjected to four-point bending. The corrugation configuration used in these models is sourced from a previous study [25]. The analysis is focused on how stress distribution changes under different load and support positions in relation to the corrugation waves, specifically on the flat or inclined folds. Additionally, the effect of the number of corrugation waves in the shear span is evaluated. The aim is to understand how these parameters influence the magnitude of transverse bending, and how this, in turn, affects the stress magnitude at potential crack initiation locations.

Four distinct support and load positions with both integer and non-integer numbers of corrugation waves, as depicted in Figure 21, are examined. Girder 1 features an integer number of corrugations per shear span, with loads and supports positioned on flat folds. Girder 2 exhibits a non-integer number of corrugations per shear span, with loads and supports also situated on flat folds. Girder 3 contains an integer number of corrugations per shear span, with loads and supports placed on inclined folds. Finally, Girder 4 displays a non-integer number of corrugations per shear span, with loads and supports arranged on inclined folds.
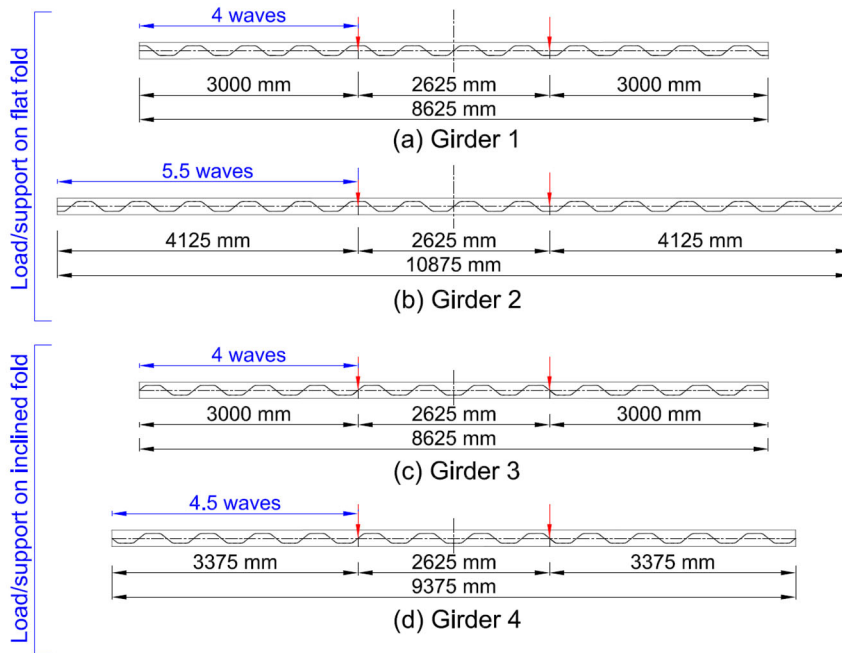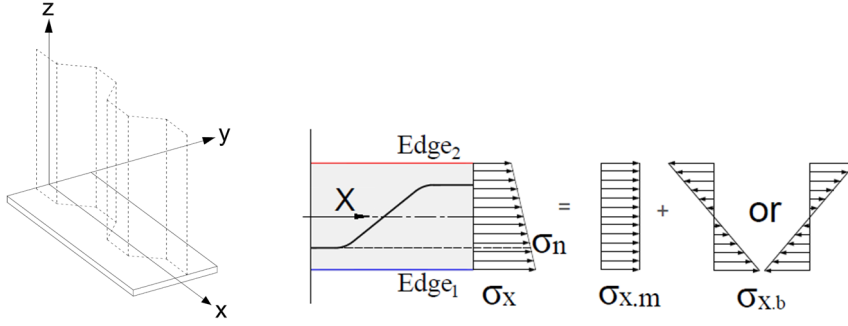

Figure 21 The configuration of corrugated web girders under study

The normal nominal stresses σ_x (Figure 22), along the two edges of the tension flange's bottom surface, are retrieved from the FEA for the four studied girders and reported in **Paper III**.

Figure 22 Representative stress components in the flanges of corrugated web beams

The results showed that both membrane and bending stresses are present in the flanges of corrugated web beams. The membrane stress ($\sigma_{x.m}$ in Figure 22) arises from primary bending around the major axis (y-axis). Bending stress ($\sigma_{x.b}$ in Figure 22) is generated by shear flow, the uneven contribution of the web to the beam's section modulus, and an unequal number of flat folds on both sides of flange X-axis. Furthermore, the magnitude of transverse bending varies based on the location of the load and support. The models proposed by Kövesdi et al. [19], discussed in the section 2.1, provide conservative estimates for these transverse bending stresses. Additionally, the findings revealed that the transverse bending from shear flow extends into the area of pure bending when the load and support are placed on inclined folds and a non-integer number of corrugations exists in the shear span. In other words, transverse bending due to shear flow is present in the pure bending region for Girder 4; however, it is absent for Girder 3.

Following these insights regarding various load effects, the next question arises: can the bending and membrane stresses be superimposed for fatigue design? This would be the case if the stress concentration factors generated at the S-point by membrane and bending stresses are comparable. To investigate this, both experimental and numerical studies are conducted to assess the impact of transverse bending on hot-spot stress at potential crack initiation locations, i.e., the S-points. Two types of loading are employed: Load Type 1 (LT1) utilizes the same configuration for Girder 4, while Load Type 2 (LT2) follows the same configuration for Girder 3. As mentioned earlier, the key distinction between these types is that transverse bending occurs in the pure bending region for LT1, whereas it is absent in LT2. The study is conducted on a duplex stainless-steel beam, with dimensions depicted in Figure 23. Fiber optics were installed to measure the strains along the two flange edges for both loading types, and hot-spot stresses were derived from strain measurements at two opposite corners within the pure bending region (S-Point1 and S-Point2 in Figure 23). The findings are summarized below, with more details available in **Paper IV**.
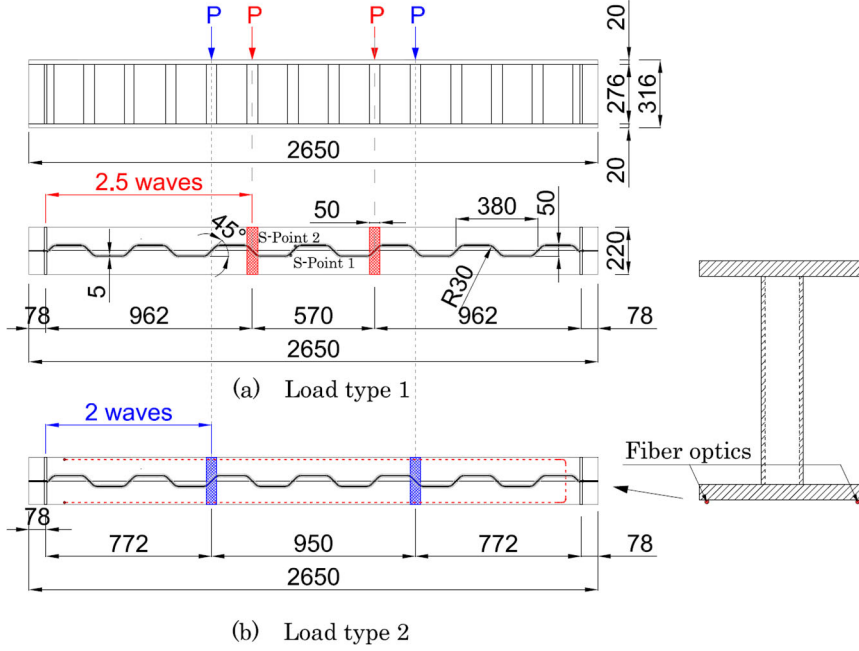
(a) Load type 1

(b) Load type 2

Figure 23 Tested beam dimensions overview

The measurements obtained from the fibres confirmed the findings of the finite element analysis (FEA), as shown in Figure 24, indicating transverse bending in the pure bending region for LT1, while no such bending was observed for LT2.
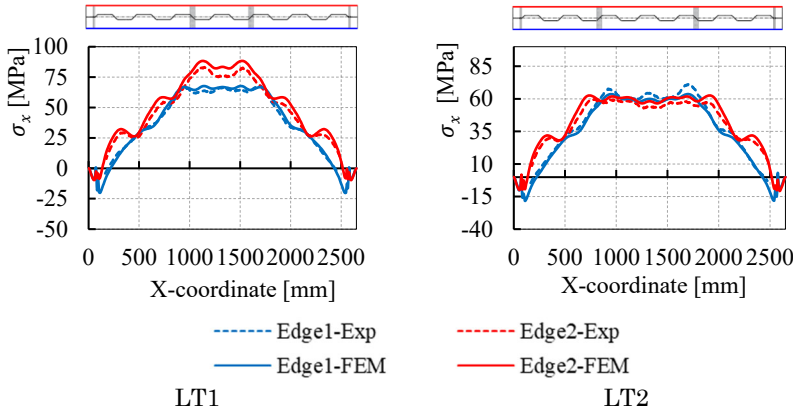

Figure 24 Stress distribution along bottom flange edges (bottom surface) from FEA and Experiment

Furthermore, both FEA and experimental results showed comparable hotspot stresses at the upper and lower corners for LT2. In contrast, LT1 exhibited a notable difference due to the presence of transverse bending, as shown in Table 8. Incorporating transverse bending into the nominal

stress calculations (i.e., σ_n in Figure 22 instead of $\sigma_{x.m}$), yields a more consistent stress concentration factor (SCF) between the two corners. This adjustment also brings the SCF values of LT1 and LT2 into closer agreement, suggesting that the same stress concentration factor can be used for both membrane and transverse bending stresses.

Table 8 Hot spot stresses and concentration factors from the experiment, including transverse bending in nominal stress

|		$\sigma_{n.exp}$ [MPa]	$\sigma_{HS.exp}$ [MPa]	SCF_{exp}
LT1	S-Point 2	61.25	83.16	1.36
	S-Point 1	57.13	76.23	1.33
LT2	S-Point 2	51.15	67.80	1.33
	S-Point 1	51.15	68.69	1.34

Since the model proposed by Kövesdi et al. [19] was found to yield conservative results for the transverse bending stress; it is proposed that this model be used when considering the load effects for the fatigue design of the flange-to-web welded detail using the nominal stress method. Specifically, the stress at the corrugation corner, as defined in Equation (3-6) is proposed to be used as the nominal stress.

$$\sigma_n = \frac{M_y}{W_y} + \frac{M_z}{W_{flange}} * \frac{a_3}{b_f} \tag{3-6}$$

Where W_y is the beam section modulus of area, neglecting the web contribution, M_z is the transverse bending moment calculated according to Kövesdi et al. (equation given in Figure 5b). W_{flange} is the flange section modulus $W_{flange} = \frac{t_f * b_f^3}{12}$.

3.4.2 Study D: Review of carbon steel fatigue tests

A total of 86 experimental data on fatigue of the flange-to-web welded detail with corrugated webs were compiled from the literature [21-28]. After removing runouts, outliers, and test specimens that endured more than 5 million cycles, a statistical analysis was performed on 68 test data points in accordance with Eurocode, as detailed by Drebenstedt & Euler [95]. The findings indicated that, irrespective of the corrugation angle, a characteristic detail category of 100 MPa is applicable, as illustrated in Figure 25.
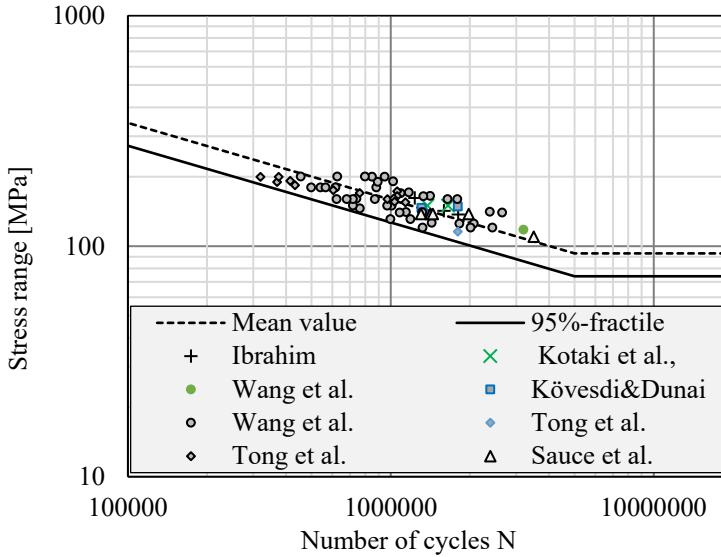
Figure 25 S-N relation of 68 test results from literature data, including those with reported fatigue cracks at S-point, excluding runouts, failure above 5 million cycles, and 1 outlier

However, previous studies have shown that the corrugation angle and bend radius have a significant impact on the fatigue strength of corrugated web girders [96]. Therefore, the compiled test results were categorized and reanalysed according to these parameters. When the results were categorized by the corrugation angle, four distinct S-N curves were established and subsequently standardized into detail categories as outlined in EN1993-1-9. The proposed detail categories based on corrugation angles are summarized in Table 9. When girders with similar corrugation angles but differing bend radii were examined, the findings did not demonstrate a strong correlation between bend radius and fatigue strength.

Table 9 Proposed detail categories for different corrugation angles

Corrugation angle	DC
$\alpha \leq 30$	125
$30 < \alpha \leq 40$	112
$40 < \alpha \leq 45$	100
$45 < \alpha \leq 60$	90

Worth mentioning here is that most of the compiled fatigue tests were conducted in setups that resulted in negligible transverse bending. Consequently, the S-N curves obtained from these tests tend to be non-

conservative unless the transverse bending effect (discussed in Section 3.4.1) is included on the load effect side.

Following the assessment of collected tests based on the nominal stress method, effective notch stress models were constructed to evaluate the applicability of the DC225 to the analysed detail. The objective is to leverage this method to gain a deeper understanding of some important parameters that are outside the available test pool, such as the effect of flange thickness and the risk of root cracking in the studied detail. Finite element models of selected tension test specimens with varying corrugation angles were developed to calculate the effective notch stress at both the weld toe and root. The tests were sourced from Wang et al. [27]. Figure 26 shows that using ENS at the weld toe reduces scatter significantly, making it an effective method for assessing the fatigue resistance of the studied detail compared to the nominal stress approach. This is seen from the reduction in standard deviation from 0.17 to 0.09 from nominal and ENS analysis, respectively.

(a) Nominal stress
Standard deviation: 0.17
No. of tests 40

(b) Effective notch stress
Standard deviation: 0.09
No. of tests 40
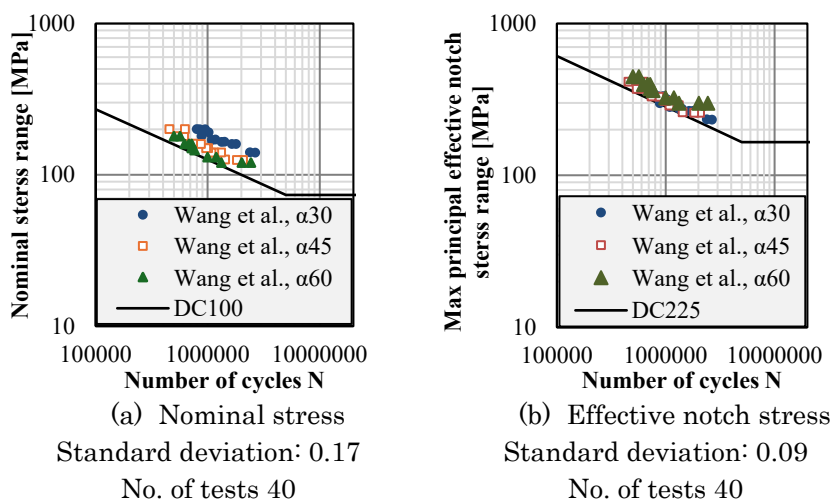
Figure 26 Fatigue life as a function of nominal stress and effective notch stress

Noting that the compiled test data include flange thicknesses varying from 6 to 20 mm, it is anticipated that larger flange thicknesses will be present in bridge girders. Therefore, the effective notch stress method was employed to investigate the influence of flange plate thickness on stress concentration. The findings, presented in Table 10, indicate that the stress concentration factor is not significantly affected by flange thickness within the tested and modeled ranges.

Table 10 Effective notch stress at the weld toe and root in the S-point area for angle α=45° and flange thickness t_f = 6 mm, 24 mm, 48 mm obtained from FE analysis

	Nominal stress [MPa]	ENS_{Toe} [MPa]	ENS_{Root} [MPa]	SCF_{Toe}	ENS_{Toe}/ ENS_{Root}
α = 45°, t_f = 6 mm	158.14	328.72	250.5	2.08	1.31
α = 45°, t_f = 24 mm	175.76	348.88	259	1.98	1.35
α = 45°, t_f = 48 mm	176.80	349.97	265.12	1.98	1.32

With reference to root cracking, the ENS analysis revealed significant stress on the root side of the detail studied, near the section passing through the S-point, suggesting a potential risk of root cracking. The modelled specimens had a weld throat thickness of 3 mm and a web plate thickness of 4 mm, resulting in a ratio $\frac{2a_w}{t_w}$ of 1.5. The ratio ENS_{Toe}/ ENS_{Root} for the three corrugation angles and the three thicknesses was approximately 1.3, unaffected by flange thickness and the corrugation angle, indicating that to avoid root cracking, the ratio $\frac{2a_w}{t_w}$ needs to be at least 1.15. Further analysis is required to confirm this conclusion. Notably, the collected tests met this ratio, except for two tests, which did not report root cracking.

3.4.3 Study E: Fatigue testing on duplex stainless steel

Following the review of the previous tests on carbon steel, an experimental program on duplex stainless-steel beams was conducted. The aim is to evaluate the fatigue behavior of stainless-steel corrugated web girders and compare it with carbon steel. This section provides a summary of the test program and test results, with more details available in **Paper VI**.

Two groups of beams with varying angles and radii were designed, manufactured, and tested under cyclic loading. A total of 15 beams were produced, comprising 7 beams in Group B and 8 in Group C. The dimensions of the tested beams and the test setup are presented in Figure 27 and Figure 28.
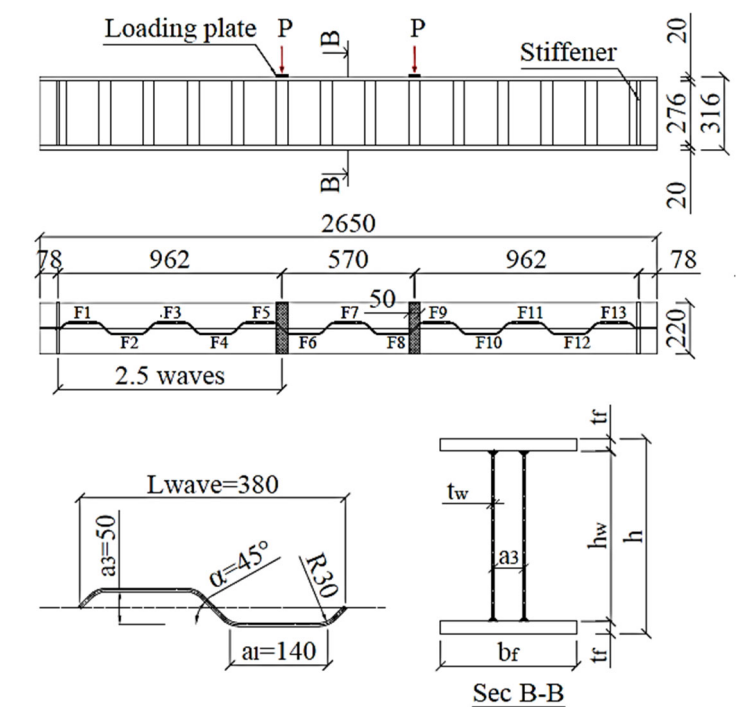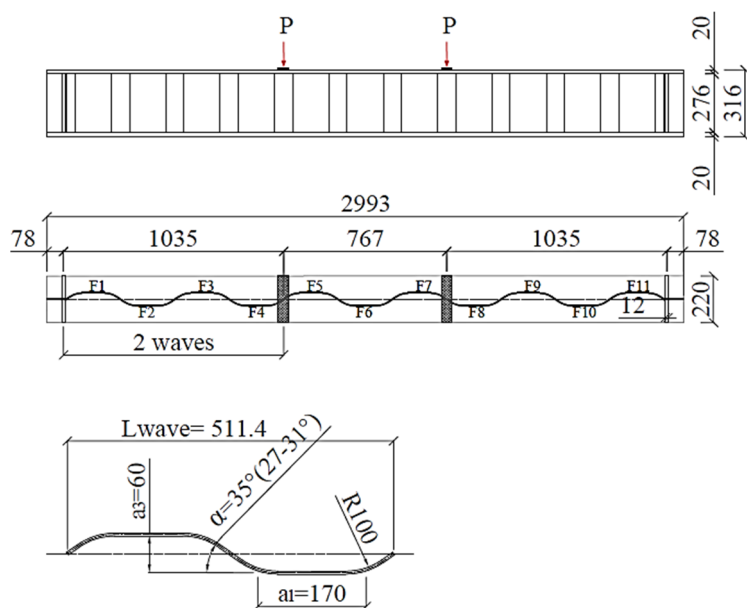
Figure 27 Dimensions and geometric notations of the tested beams

Figure 28 Testing setup

The beams were subjected to four-point bending. Strain gauges were installed to measure the membrane and bending stresses, as well as to monitor crack development. Additionally, strain gauges were placed to estimate the hot spot stress at two opposite corners within the pure bending region of one beam from each series. The testing commenced with gradual load increases for one beam in each series to ensure that elastic stress ranges were maintained. The test results indicated small deviations between the measured and calculated stresses using beam theory, with less than 3% transverse bending in relation to the membrane stress observed at the crack initiation location due to the wide flange in relation to the corrugation depth. Consequently, the calculated membrane stresses were deemed suitable for use in the fatigue evaluation with the nominal stress method. Following this, cyclic loading was applied with a stress ratio of 0.1. The fatigue test matrix is presented in Table 11.

Table 11 Summary of test program

Beam	P_{max} [kN/point]	P_{min} [kN/point]	P_{max}/P_{yield} [-]	$\Delta\sigma_m$ [MPa]
B1	300	30	52%	185.7
B2	300	30	52%	185.7
B3	300	30	52%	185.7
B4	300	30	52%	185.7

B5	220	22	38%	136.2
B6	220	22	38%	136.2
B7	220	22	38%	136.2
C1	205	20.5	36%	136.5
C2	205	20.5	36%	136.5
C3	205	20.5	36%	136.5
C4	240	24	42%	159.8
C5	205	20.5	36%	136.5
C6	250	25	43%	166.4
C7	250	25	43%	166.4
C8	240	24	42%	159.8

Additionally, two finite element models were developed for the two tested beam series. These models were validated against the test measurements and used to extract the hot spot stress and effective notch stresses, allowing for a comprehensive evaluation of the results using the ENS and HSS methods.

The tested beams exhibited two main types of fatigue cracking: web cracking and flange cracking. Beams B1 and B2 displayed web cracking within the shear span, as illustrated in Figure 29. The web weld lines of the remaining beams were treated with HFMI, which subsequently led to the development of flange cracks that initiated at the S-point, as depicted in the same figure.
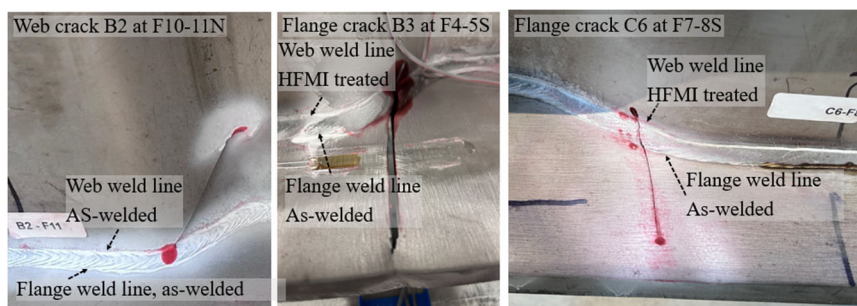
Figure 29 Developed fatigue cracking modes

Some flange cracks in group B appeared outside the pure bending region. This was believed to occur due to the geometry of the test specimen, characterized by a thin and short web in relation to a wide and thick flange—not typical for bridge girders—which needed further insight.

Such dimensions led to elevated ENS/HSS at specific corners in the shear span, which was numerically observed in both Group B and C. To explore this phenomenon further, a numerical study was conducted for
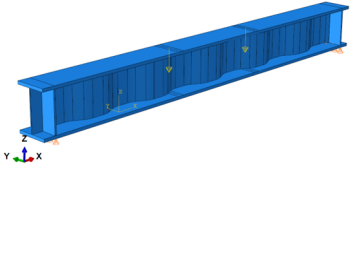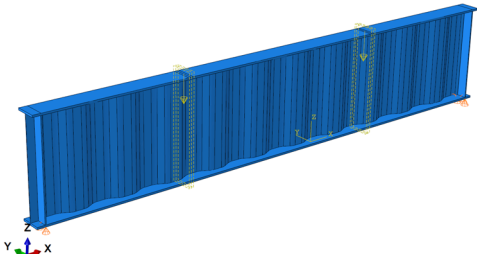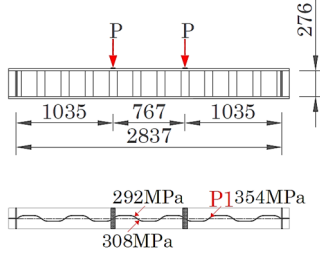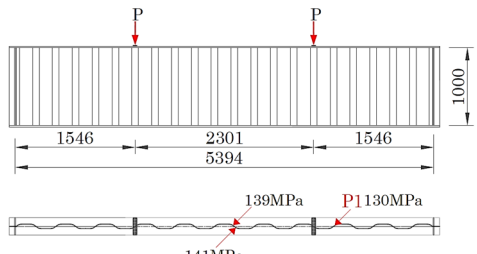
Group C by increasing the web height to 1m and the beam length to 5.4m. ENS values were extracted from finite element analysis at two opposite corners in the pure bending region and the corner with elevated ENS in the shear span (point P1 in Table 12).

The results are presented in Table 12 which shows that, for the original test specimen size, ENS outside the pure bending area is higher than inside, and the stress concentration factor varies. As the specimen size increases, the ENS in the pure bending area becomes larger than that in the shear span, with closer stress concentration factors. This suggests that this effect is linked to the test specimen geometry, so—in this study—only cracks in the pure bending area are evaluated using the nominal stress method. However, this needs further investigation to find out at what geometrical parameters these local effects occur.

With hotspot and effective notch stress methods, all flange cracks — irrespective of location —are assessed. Also, the points with high ENS in the shear span were treated with HFMI for Group C beams, while they were kept as-welded in Group B. Consequently, cracks appeared at these locations in Group B beams but not in Group C beams.

Table 12 Specimen size effect. Applied load 240kN/point.

276cm deep, 2.8m long	1m deep, 5.4m long
$SCF_{ENS.pure\ bending\ region}=1.74$	$SCF_{ENS.pure\ bending\ region}= 1.74$
$SCF_{ENS.P1}=2.4$	$SCF_{ENS.P1}=1.78$

The statistical evaluation conducted on cracks developed in the pure bending region with the nominal stress method is illustrated in Figure 30. Group B's thirteen cracks yielded DC104, while Group C's seven cracks yielded DC127, which can be rounded to DC100 and DC125 standards in EN1993-1-9. This is in line with previously proposed detail

categories for carbon steel beams based on the corrugation angles discussed in Section 3.4.2 and presented in Table 9.

Group B
α= 45° (no. of points=13)
Standard deviation= 0.04
DC= 104MPa

Group C
α= 27°-31° (no. of points=7)
Standard deviation= 0.06
DC= 127MPa
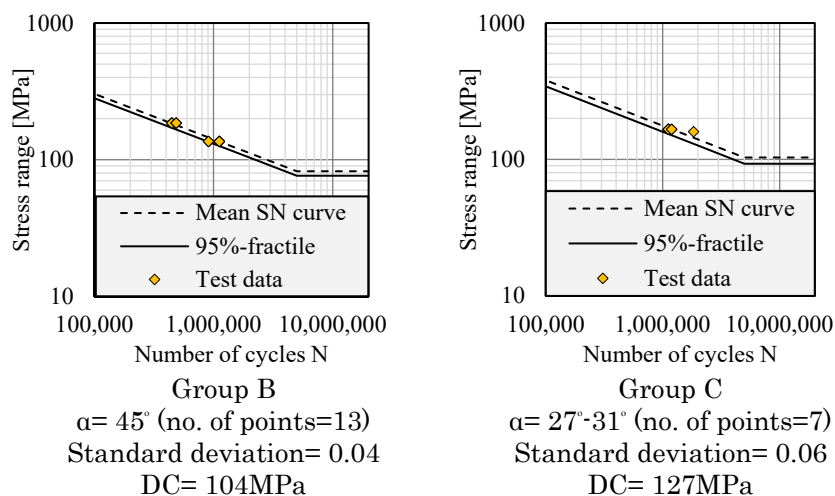
Figure 30 Statistical evaluation of the test data with the nominal stress method

Figure 31 further presents previous fatigue test results on specimens made of carbon steel with a corrugation angle of 45°, alongside data from stainless steel Group B, showing the mean and ±2STD. A similar comparison is made for Group C with a 30° angle. The figure shows that the stainless-steel results are in good agreement with the earlier carbon steel data.
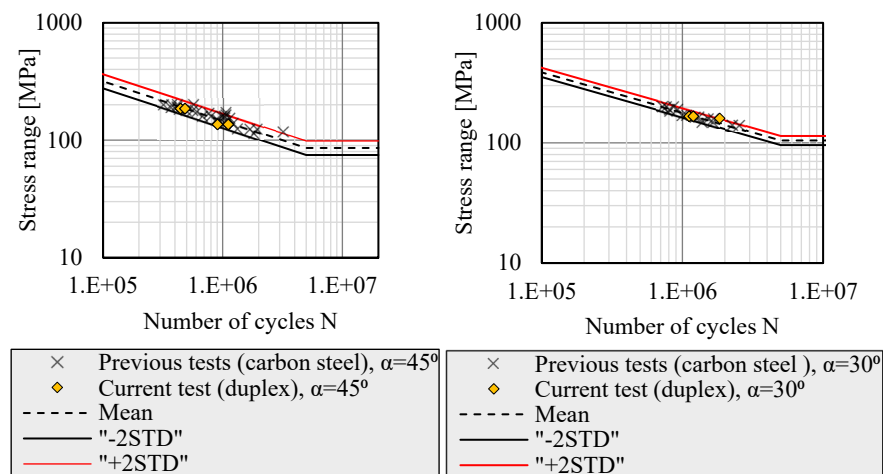
Carbon steel data sourced from Wang et al. [27], Tong et al. [28], and Wang et al. [58]

Carbon steel data sourced from Kotaki et al. [24] and Wang et al. [27]

Figure 31 Previous fatigue tests on carbon steel compared to current testing on duplex stainless-steel EN1.4162

The assessment of all flange cracks that developed in both the pure bending region and the combined shear and bending region using HSS and ENS methods is presented if Figure 32. With reference to the HSS method, all test results lie above the DC100 curve. However, the DC100 appears overly conservative for Group C, where the notch effect is less significant than in Group B. With reference to the ENS method, all test data points lie above the DC225 fatigue class recommended by IIW for effective notch stress in as-welded conditions when the evaluation is conducted with max principal stress component, indicating that this method can predict the fatigue life of the flange-to-web welded detail in corrugated web girders.
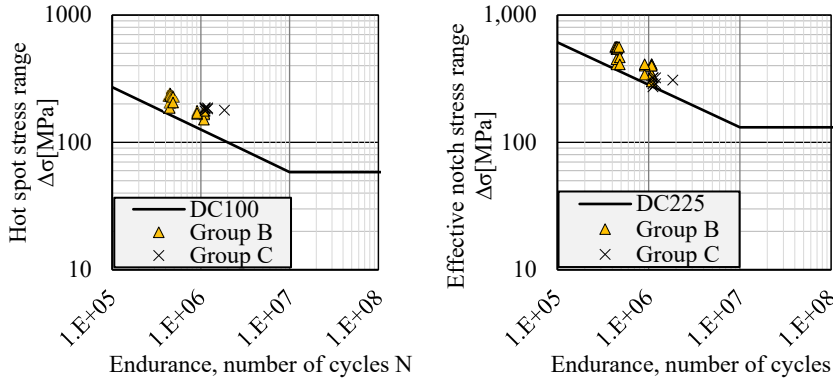
Figure 32 Experimental data with HSS/ENS from FE-analysis. Maximum principal stress component

The evaluation of the developed web cracks is carried out using the ENS method alongside the EN1993-1-9 approach for combined stress range. This approach estimates fatigue life by assuming that the total damage from shear and bending equals one. The results are illustrated in Figure 33, with both methods providing conservative outcomes for the tested beams. It is worth mentioning here that these web cracks are similar to those recently reported by Zuo et al. [59], as discussed in Section 2.1, highlighting the importance of accounting for web cracking in the design of these beams.
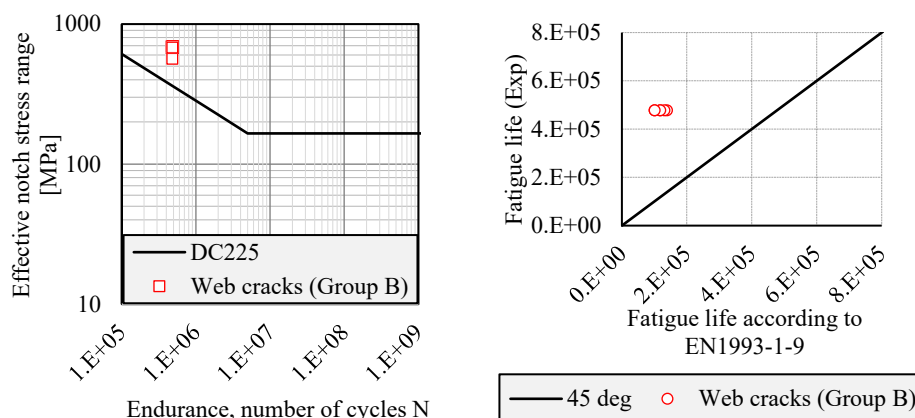
Figure 33 Assessment of fatigue web cracks in beams B1&B2

3.4.4 Further observations from fatigue testing

During testing, two additional cracking modes were observed in Group C beams. Beams C1 and C2 developed cracks along the flange width above the support, whereas beam C8 exhibited two cracks on the compression side within the pure bending region, specifically at F5-6N and F7-8S. These cracking modes are illustrated in Figure 34.

Figure 34 Fatigue cracking at the support in beams C1&C2, and on the compression side in beam C8

The dimensions of the delivered beams of Group C showed some deviation from the designed values. For instance, in beams C1 and C2, the measured distance between the two support stiffeners was approximately 30 mm different from the distance between the supports

in the testing machine. This eccentricity was incorporated into the finite element analysis, which revealed higher stress in these localized areas (Figure 34), which, combined with the complex welded detail and high residual stresses at the support location, contributed to the observed cracking. To mitigate this type of cracking in the other beams, pairs of beams closest in length were selected for simultaneous testing (C4 and C8, C6 and C7, C3 and C5), and the distance between the supports in the testing machine was adjusted accordingly.

The crack on the compression side of beam C4 was attributed to tensile stress resulting from residual stress, combined with poor weld quality at this location, as shown in Figure 34. This crack was detected simultaneously with a surface crack on the tension side at F7-8S that has been included in the statistical analysis presented above (Figure 30).

Chapter 4

4 Conclusions and future work

4.1 Conclusions

The present study aimed firstly to investigate the viability of stainless-steel corrugated web I-girders as a sustainable alternative to traditional carbon steel flat web I-girders in composite road bridges. Secondly, it supports the implementation of this concept by examining the flange buckling problem and conducting a fatigue assessment of the flange-to-web welded detail at the corrugation corners.

A design optimization tool was developed and employed to evaluate the concept. Parametric finite element analyses were conducted to investigate the flange buckling problem. For fatigue, a combination of numerical and experimental approaches was used to study load effects relevant to the fatigue design of the flange-to-web welded detail. Additionally, reported fatigue test data on the same detail in carbon steel were compiled and statistically evaluated. Finally, an experimental program was carried out to assess the fatigue strength of the detail in duplex EN 1.4162 stainless steel. Based on the findings, the main conclusions—aligned with the research objectives—are summarized below.

Concept evaluation
The following conclusions were drawn from Study **A** on the evaluation of the stainless-steel corrugated web girder concept for composite road bridges:

- The result showed that the stainless-steel corrugated concept can considerably reduce the high initial investment costs associated with using stainless steel, bridging the cost gap between carbon and stainless steel, while still preserving the long-term benefits of stainless steel, including corrosion resistance and low maintenance requirements. It also outperformed the conventional flat web carbon steel design in terms of weight, life cycle cost, and environmental impact.
- Optimization design solutions varied depending on the selected optimization objective. For stainless steel, material usage strongly influenced both cost and life cycle environmental impact. Therefore, when the goal is to minimize weight, cost (LCC or

investment), or environmental impact, the algorithm prioritizes material reduction. In contrast, for carbon steel, painting costs are considerable (20–29% of investment cost and 36–55% of total LCC), making the minimization of painted surface area a key objective when cost is the primary concern. However, if weight or environmental impact is prioritized, the algorithm also focuses on reducing material in the carbon steel design.

- When the cost ratio between S355 and EN1.4162 is 3, the stainless-steel corrugated web concept was achieved with a modest increase in investment cost (1–11%) compared to the traditional flat web design. This is primarily attributed to the weight savings achieved in the corrugated web design and eliminating the need for painting. Across the studied cases, weight savings ranged from 20–38%. Eliminating the need for grinding, decreasing welding costs as fewer cross beams, stiffeners, and thinner steel plates are used, further contributes to lowering the production cost of the EN1.4162 corrugated web design.

- With reference to LCC, besides the above-mentioned points, the studied concept reduces maintenance costs by eliminating the need for painting activities for steel works. Eliminating paint repairs also removes the accompanied traffic disruption expenses. In the studied cases, LCC savings ranged from 20–49%.

- Limiting the maximum girder height reduces the benefits. A height limit of 1.5 m increased the investment cost gap to 26% and reduced the LCC saving to 5%. With increased height allowances, however, increasing the depth of stainless-steel corrugated webs allows for greater material savings without incurring the additional painting costs associated with the larger surface areas of the carbon steel option.

- The influence of ADT and N_{obs} on design outcomes varies. Raising N_{obs} means moving the governing design limit state from the ultimate limit state to the fatigue limit state, which limits the benefits of the higher-strength stainless steel material. At the same time, ADT rises as N_{obs} increases, which in turn increases user costs. These user costs depend on the expected repair work closing time, ranging from no traffic diversions to several weeks or months. In the three scenarios considered, the studied concept demonstrated potential LCC savings of 43–49%.

- LCC savings were comparable for both short and long spans, ranging from 20–26% for long-span bridge cases and 18–22% for short-span cases.

- The environmental impact, measured in Global Warming Potential (GWP), was 32–42% lower than that of the traditional concept. Material production was the main contributor to environmental impact, with stainless steel having a significantly lower unit GWP than S355 carbon steel (1.7 kg CO_{2eq}/kg

compared to 2.63 kg CO_{2eq}/kg). Variations in data sources will influence the calculated benefits.

- The weight saving achieved by using higher-strength carbon steel material (S460) is partially offset by its higher material cost. When the fatigue limit state governed the design, the life cycle costs of both S355 and S460 were comparable, both being higher than that obtained with corrugated web design.

Flange buckling

The conclusions drawn from Study **B** on the flange buckling problem are summarized below:

- A comparison of the numerical results with three models for the flange buckling resistance of carbon steel corrugated web girders—namely EN1993-1-5, DASt-Richtlinie 015, and the model proposed by Jager et al.—showed that these models are nonconservative when applied to duplex 1.4162. Both the elastic buckling coefficient (K_σ) and the buckling reduction factor (ρ) obtained from these models showed poor agreement with the results of the numerical analysis.
- A new buckling curve, along with an equation for calculating the elastic buckling coefficient, has been proposed. This proposal showed satisfactory results across observed failure modes. Nevertheless, given the complexity of the problem and the various influencing factors, a degree of underestimation of flange buckling resistance was deemed acceptable.
- The proposed buckling curve yields a relative slenderness limit of $\bar{\lambda}_p \leq 0.4$ for duplex trapezoidal corrugated web beams. Consequently, a cross-sectional class 4 limit of $c_f/t_f > 11.36\varepsilon\sqrt{k_\sigma}$.

Fatigue assessment

The conclusions drawn from Studies **C**, **D**, and **E** regarding the fatigue assessment of the flange-to-web welded detail are summarized below:

- Analysis of the compiled fatigue test data for carbon steel corrugated web members revealed that the fatigue life of the flange-to-web welded detail is strongly affected by the corrugation angle. This allowed for assigning different detail categories based on the corrugation angle: DC125 for angles equal to or smaller than 30◦, DC112 for angles between 30◦ and 40◦, DC100 for angles between 40◦ and 45◦, and DC90 for angles between 45◦ and 60◦.
- Both experimental and finite element analyses showed that transverse bending affects the stress magnitude at the S-point (the crack initiation location), highlighting the need to account for it in fatigue design of corrugated web girders.
- The majority of the compiled fatigue tests were conducted in setups with negligible transverse bending. As a result, the S-

    N curves derived from these tests tend to be non-conservative unless transverse bending is included on the load effect side.

- The evaluation of test results from both carbon and stainless-steel specimens with different corrugation geometries using the effective notch stress method showed that DC225, based on the maximum principal effective notch stress component at the weld toe (S-point), can predict the fatigue life of the flange-to-web welded detail in corrugated web girders.
- Regarding the flange thickness effect in the studied detail, the limited ENS analysis, which included three different flange thicknesses, indicated that the flange thickness does not significantly impact the fatigue strength of the studied detail.
- Regarding root cracking, the high stresses observed at the root side of the flange-to-web detail in the ENS analysis suggest that root cracking may occur if the ratio between the total weld throat thickness to the web thickness $(2a_w/t_w)$ is less than 1.15.
- The tested stainless-steel girders exhibited similar fatigue strength to their carbon steel counterparts. Beams with a 45° corrugation angle conformed to DC100, while those with around 30° angle conformed to DC125.
- DC100 for the hot spot stress method using maximum principal stress provided a conservative estimation of the fatigue strength of the tested beams.
- It goes without saying that web cracking should also be checked in beams with corrugated webs, as these webs transfer both shear and normal stresses at the interface between the web and the flange.

The research presented in this thesis showed promising potential for the stainless-steel corrugated web concept in terms of material usage, life cycle cost, and environmental impact. It also addressed two key design aspects, bringing the use of stainless steel in future bridge projects closer to practical application.

4.2 Suggestions for future research

A comprehensive analysis examining the impact of various geometric parameters on the stress concentration in beams with corrugated webs would be advantageous in supporting and validating an extension of the proposed detail categories to girders featuring geometric parameters beyond those included in the collected tests, such as thicker webs and larger corrugation angles.

    Further research is needed to understand how the specimen geometrical parameters influence local distortions and fatigue performance of corrugated web girders.

    One design aspect not addressed in this thesis is the patch loading resistance. The lightweight corrugated web girder concept is particularly advantageous for bridges erected by launching, where girders are

subjected to concentrated transverse loads (patch loads). A draft for the new Eurocode [97] provides a patch loading model based solely on the web's contribution. However, previous research has shown that the flange also contributes to the resistance capacity [98] [99] [100]. Furthermore, limited studies have investigated how the loading length affects the capacity [101]. Therefore, a less conservative prediction model for the patch load resistance of corrugated web beams made of both carbon steel and stainless steel is needed.

The corrugation parameters influence structural capacity in different ways; for example, increasing the corrugation angle enhances shear capacity but reduces fatigue resistance. With the developed models for flange buckling and fatigue design, together with existing models for other aspects, a parametric design optimization study —as in Paper I— can be conducted to identify optimal corrugation parameters with respect to structural performance and cost efficiency.

References

[1]   United Nations. (2015). Transforming our World: The 2030 Agenda for Sustainable Development. *United Nations*.
        Retrieved from: https://sustainabledevelopment.un.org/

[2]   European Commission. (2016). Communication from the Commission on Next steps for a sustainable European future European action for sustainability. *European Commission*.
        Retrieved from: https://eur-lex.europa.eu

[3]   Baddoo, N.R., Kosmač, A. (2010). Sustainable Duplex Stainless Steel Bridges.
        Retrieved from: https://www.shortspansteelbridges.org

[4]   Kuhlmann, U., Feldmann, Markus, Naumes, Johannes, Martin, Pierre-Olivier, Galéa, Yvan, Johansson, Bernt, Collin, Peter, Eriksen, Jörgen, Degée, Hervé, Hausoul, Nicolas, Chica, José, Meno, Sandra, Raoul, Joël, Davaine, Laurence, Petel, Aude (2008). COMBRI DESIGN MANUAL Part II: State-of-the-Art and Conceptual Design of Steel and Composite Bridges.

[5]   Collin, P., Johansson, B., Sundquist, H. (2008). Steel concrete composite bridges. *Structural design & bridges, KTH, Stockholm*.
        Retrieved from: https://libris.kb.se/bib/11416797

[6]   Wahlsten, J., Heshmati, Mohsen, Al-Emrani, Mohammad (2018). Sustainable Infrastructure through Increased Use of Stainless Steel.
        https://research.chalmers.se/project/8144

[7]   Rossi, B. (2014). Discussion on the use of stainlesssteel in constructions in view of sustainability. *Thin-Walled Structures*, *83*, 182-189.
        http://dx.doi.org/10.1016/j.tws.2014.01.021

[8]   Karabulut, B., Ferraz, G., Rossi, B. (2021). Lifecycle cost assessment of high strength carbon and stainless steel girder bridges. *Journal of Environmental Management*, *277 (111460)*.
        https://doi.org/10.1016/j.jenvman.2020.111460

[9]   Zilli, G., Fattorini, F., Maiorana, E. (2008). Application of duplex stainless steel for welded bridge construction in aggressive environment. *The International Conference Duplex 2007, Grado, Italy*.
        https://www.researchgate.net/publication/265668326

[10]   Säll, J., Tiderman, A. (2013). Maintenance-free material in bridge superstructures: Benefits in a cost- and environment prospective in use of stainless steel and directly molded durable concrete. *KTH Royal Institute of Technology*.
        Retrieved from: https://kth.diva-portal.org/

[11]   Boutillon, L., Combault, Jacques, Ikeda, Shoji, Imberty, Florent, Mori, Takuya, Nagamoto, Naoki, Novak, Balthasar, Saito, Kimio. (2015). Corrugated-steel-web bridges.
Retrieved from: https://shop.fib-international.org/publications/

[12]   Wilson, A.D. Advances in High Performance Steels for Highway Bridges. *National Steel Bridge Alliance (NSBA) White Paper*.

[13]   Gedge, G. Stainless Steel In Bridge Design. *Arup Materials Consulting, Solihull, UK*.

[14]   Amani, M., Al-Emrani, Mohammad, Flansbjer, Mathias. (2023). Shear Behavior of Stainless Steel Girders with Corrugated Webs. *Journal of Constructional Steel Research*, *210*.
https://doi.org/10.1016/j.jcsr.2023.108086

[15]   Jáger, B., Dunai, L., Kövesdi, B. (2017). Flange buckling behavior of girders with corrugated web Part II: Numerical study and design method development. *Thin-Walled Structures*, *118*, 238-252.
https://doi.org/10.1016/j.tws.2017.05.020

[16]   Johansson, B., Maquoi, R.,Sedlacek, G.,Müller, C., Beg,D. . (2007). Commentary and Worked Examples to EN 1993-1-5 "Plated Structural Elements". *European Commission Joint Research Centre*.

[17]   EN1993-1-9. (2005). Eurocode 3: Design of steel structures- Part 1-9: Fatigue.

[18]   prEN1993-1-9:2023. Eurocode 3 — Design of steel structures — Part 1.9: Fatigue.

[19]   Kövesdi, B., Jáger, B., Dunai, L. (2012). Stress distribution in the flanges of girders with corrugated webs. *Journal of Constructional Steel Research*, *79*, 204-215.
https://doi.org/10.1016/j.jcsr.2012.07.023

[20]   Abbas, H.H., Sause, R., Driver, R.G. (2007). Analysis of flange transverse bending of corrugated web I-girders under in-plane loads. *Journal of structural engineering*, *133 (3).* 347–355.
https://doi.org/10.1061/(ASCE)0733-9445(2007)133:3(347)#

[21]   Ibrahim, S.A., El-Dakhakhni, W.W., Elgaaly, M. (2006). Fatigue of Corrugated-Web Plate Girders: Experimental Study. *Journal of Structural Engineering*, *132 (9).* 1371-1380.
https://doi.org/10.1061/(asce)0733-9445(2006)132:9(1371)#

[22]   Ibrahim, S.A.-B. (2001). Fatigue analysis and instability problems of plate girders with corrugated webs. *Drexel University*.
https://doi.org/10.17918/00001482

[23]   Sause, R., Abbas, H.H., Driver, G.R., Anami, K., Fisher, J.W. (2003). Fatigue Resistance of Corrugated Web Girders. *ATLSS Reports. Paper 246.*

http://preserve.lehigh.edu/engr-civil-environmental-atlss-reports/246

[24]   Kotaki, N., Ichikawa, A., Sasaki, E., Miki, C., Hosaka, T. (2003). Proposal of Ripple Web Bridge and Its Fatigue Strength. *Journal of the Japan Society of Civil Engineers*. https://doi.org/10.2208/jscej.2004.766_233

[25]   Kövesdi, B., Dunai, L. (2014). Fatigue life of girders with trapezoidally corrugated webs: An experimental study. *International Journal of Fatigue*, *64*, 22-32. https://doi.org/10.1016/j.ijfatigue.2014.02.017

[26]   Xu, J., Sun, H., Cai, S., Sun, W., Zhang, B., . (2019). Fatigue testing and analysis of I-girders with trapezoidal corrugated webs. *Engineering Structures*, *196*. https://doi.org/10.1016/j.engstruct.2019.109344

[27]   Wang, Z., Wang, Q. (2014). Fatigue assessment of welds joining corrugated steel webs to flange plates. *Engineering Structures*, *73*. http://dx.doi.org/10.1016/j.engstruct.2014.04.041

[28]   Tong, L., Zhao, Z., Zuo, G., Wang, H., Pan, C. (2024). Experimental study on fatigue behavior of trapezoidal corrugated-web girders based on T-section members. *Engineering Structures*, *298*. https://doi.org/10.1016/j.engstruct.2023.117078

[29]   Mameng, S.H., Backhouse, A., , McCray, J., Gedge, G. . (2018). Experience of duplex stainless steels as structural materials for bridges. *9th International Symposium on Steel Bridges*. https://iopscience.iop.org/article/10.1088/1757-899X/419/1/012018

[30]   Karabulut, B., Lombaert, G., Debruyne, D., Rossi, B. (2018). Numerical Investigations on the Fatigue Life of Lean Duplex Transverse Stiffeners in Bridges. *The 18th International Conference on Experimental Mechanics*. https://doi.org/10.3390/ICEM18-05278

[31]   Jáger, B., Dunai, L., Kövesdi, B. (2017). Flange buckling behavior of girders with corrugated web Part I: Experimental study. *Thin-Walled Structures*, *118*, 181-195. https://doi.org/10.1016/j.tws.2017.05.021

[32]   Elamary, A.S., Alharthi, Yasir.M., Hassanein, Mostafa F., Sharaky, Ibrahim.A. (2022). Trapezoidally corrugated web steel beams loaded over horizontal and inclined folds. *Journal of Constructional Steel Research*, *192*. https://doi.org/10.1016/j.jcsr.2022.107202

[33]   Elgaaly, M., Seshadri, Anand (1998). Depicting the behavior of girders with corrugated webs up to failure using non-linear finite element analysis. *Advances in Engineering Software*, *29 (3-6)*. https://doi.org/10.1016/S0965-9978(98)00020-9

References

[34]   Pasternak, H., Hannebauer, Dina. (2004). Träger mit profilierten Stegen.
        Retrieved from: https://www.researchgate.net/publication/342644235

[35]   Leblouba, M., Karzad, Abdul Saboor, Tabsh, Sami W., Barakat, Samer. (2022). Plated versus Corrugated Web Steel Girders in Shear: Behavior, Parametric Analysis, and Reliability-Based Design Optimization. *Buildings*, *12 (12).* 2046.
        https://doi.org/10.3390/buildings12122046

[36]   Elamary, A.S., Saddek, Amr B., Alwetaishi, Mamdooh. (2017). Effect of corrugated web on flexural capacity of steel beams. *International Journal of Applied Engineering Research*, *12 (4).* 470-481.

[37]   Elgaaly, M. (1997). Bending strength of steel beams with corrugated webs. *Journal of structural engineering*, *123 (6).*
        https://doi.org/10.1061/(ASCE)0733-9445(1997)123:6(772)#

[38]   Inaam, Q. and A. Upadhyay. (2022). Accordion effect in bridge girders with corrugated webs. *Journal of Constructional Steel Research*, *188*.
        https://doi.org/10.1016/j.jcsr.2021.107040

[39]   Kövesdi, B., Jáger, B., Dunai, L. (2016). Bending and shear interaction behavior of girders with trapezoidally corrugated webs. *Journal of Constructional Steel Research*, *121*, 383-397.
        http://dx.doi.org/10.1016/j.jcsr.2016.03.002

[40]   Abbas, H.H., Sause, R, Driver, R.G. (2006). Behavior of Corrugated Web I-Girders under In-Plane Loads. *Journal of Engineering Mechanics*, *132 (8).* 806-814.
        https://doi.org/10.1061/(ASCE)0733-9399(2006)132:8(806)#

[41]   EN1993-1-5. (2006). Eurocode 3 - Design of steel structures - Part 1-5: Plated structural elements.

[42]   Baláž, I., Koleková, Y. (2012). Influence of Transverse Bending Moment in the Flange of Corrugated I-Girders. *Procedia Engineering*, *40*, 26-31.
        https://www.researchgate.net/publication/257725189

[43]   Al-Emrani, M., ÅKESSON, BJÖRN (2020). Steel Structures Report ACE2020:13. *Chalmers University of Technology*.
        http://bit.ly/3H3T3tv

[44]   Saddek, A., Tohamy, Sedky, Elsayed, Amr, Drar, Ahmed Attia M. (2021). Numerical Study of Flange Buckling Behavior of High-Strength Steel Corrugated Web I-Girders. *Journal of Engineering Sciences Assiut University Faculty of Engineering*, *49 (1).* 85-106.
        DOI: 10.21608/jesaun.2021.55553.1025

[45]   Johnson, R.P., Cafolla, J. (1997). Local flange buckling in plate girders with corrugated webs.
        https://doi.org/10.1680/istbu.1997.29304

[46]   Watanabe, K., & Kubo, M. . (2006). In-plane bending capacity of steel girders with corrugated web plates. *Journal of Structural Engineering (JSCE)*.
https://doi.org/10.2208/jsceja.62.323

[47]   Nie, J.-G., Zhu, Li, Tao, Mu-Xuan, Tang, Liang. (2013). Shear strength of trapezoidal corrugated steel webs. *Journal of Constructional Steel Research*, *85*, 105-115.
http://dx.doi.org/10.1016/j.jcsr.2013.02.012

[48]   Leblouba, M., Barakat, Samer, Altoubat, Salah, Junaid, Talha M., Maalej, Mohamed. (2017). Normalized shear strength of trapezoidal corrugated steel webs. *Journal of Constructional Steel Research*, *136*, 75-90.
http://dx.doi.org/10.1016/j.jcsr.2017.05.007

[49]   Moon, J., Yi, Jongwon, Choi, Byung H., Lee, Hak-Eun (2009). Shear strength and design of trapezoidally corrugated steel webs. *Journal of Constructional Steel Research*, *65*, 1198–1205.
https://doi.org/10.1016/j.jcsr.2008.07.018

[50]   Sause, R., Braxtan, Thomas N. . (2011). Shear strength of trapezoidal corrugated steel webs. *Journal of Constructional Steel Research*, *67*, 223–236.
https://doi.org/10.1016/j.jcsr.2010.08.004

[51]   Zhang, B., Yu, Jiangjiang, Chen, Weizhen, Wang, Hui, Xu, Jun. (2020). Stress states and shear failure mechanisms of girders with corrugated steel webs. *Thin-Walled Structures*, *157*.
https://doi.org/10.1016/j.tws.2020.106858

[52]   Al-Emrani, M., Amani, M., Björnstedt, P., Borg, P., Forsgren, E., Hedegård, J., Hällmark, R., Hlal, F., Janiak, P., Lundstjälk, A, Nilsson, P., Persson, L., Trydell, K., Zachrisson, J., Zamiri, F. (2022). SUNLIGHT – Sustainable, maintenance-free and lighter beams for stronger Swedish infrastructure.

[53]   Hlal, F., Al-Emrani, Mohammad, Amani, Mozhdeh. (2022). Preliminary Study on Plate Girders with Corrugated Webs. Report ACE 2022:3., *Chalmers University of Technology*.
https://research.chalmers.se/publication/530413

[54]   Denan, F., Osman, Mohd, Saad, Sariffuddin. (2010). The study of lateral torsional buckling behaviour of beam with trapezoid web steel section by experimental and finite element analysis. *International Journal of Research and Reviews in Applied Sciences (IJRRAS)*, *2 (3)*. 233–240.

[55]   Moon, J., Yi, Jong-Won, Choi, Byung H., Lee, Hak-Eun. (2009). Lateral–torsional buckling of I-girder with corrugated webs under uniform bending. *Thin-Walled Structures*, *47 (1)*. 21-30.
https://doi.org/10.1016/j.tws.2008.04.005

References

[56] EN1993-1-4. (2021). Amendment to Stainless steel design rules in Eurocode SS-EN 1993-1-4.

[57] Hlal, F., Al-Emrani, M. (2024). Load effects in beams with corrugated webs: Numerical study. *Nordic Steel Construction Conference 2024 (NSCC 2024), The Swedish Institute of Steel Construction.*
https://doi.org/10.5281/zenodo.12210008

[58] Wang, Z., Tan, L., Wang, Q. (2013). Fatigue strength evaluation of welded structural details in corrugated steel web girders. *International Journal of Steel Structures, 13 (4).* 707-721.
https://doi.org/10.1007/s13296-013-4012-z

[59] Zuo, G., Tong, L., Zhao, Z., Wang, H., Shi, W., Yan, Y. . (2025). Experimental study on fatigue strength of trapezoidal corrugated-web steel girders based on hot spot stress method. *Thin-Walled Structures, 208.*
https://doi.org/10.1016/j.tws.2024.112814

[60] Baddoo, N. (2017). Design Manual for Structural Stainless Steel. *SCI, Silwood Park, Ascot.*

[61] Lho, S.-H., Lee, Chang-Hwan, Oh, Jin-Tak, K. Ju, Young, Kim, Sang-Dae. (2014). Flexural capacity of plate girders with very slender corrugated webs. *International Journal of Steel Structures, 14 (4).* 731-744.
https://link.springer.com/article/10.1007/s13296-014-1205-z

[62] Ning, P., Tong, L., Zhao, Z., Wang, H., Pan, C., Zhu, X. (2025). Residual stress distributions of trapezoidal corrugated web I-members: Experimental and numerical study. *Journal of Constructional Steel Research, 225.*
https://doi.org/10.1016/j.jcsr.2024.109188

[63] ISSF. (2019). The stainless-steel family. International Staineless Steel Forum.
https://worldstainless.org/

[64] Trafikverket. (2019). Krav Brobyggande. TDOK 2016:0204 Version 3.0.

[65] Yang, X. (2010). Engineering optimization: An introduction with metaheuristic applications. *University of Cambridge.*

[66] Chalouhi, E.K. (2022). Optimal design solutions of road bridges considering embedded environmental impact and cost. *PhD thesis, KTH Royal Institute of Technology.*

[67] Skoglund, O., Leander, John, Karoumi, Raid. (2020). Optimizing the steel girders in a high strength steel composite bridge. *Engineering Structures, 221.*
https://doi.org/10.1016/j.engstruct.2020.110981

[68]   Bozorg-Haddad, O., Solgi, Mohammad, A. Loaiciga, Hugo. (2017). Meta-Heuristic and Evolutionary Algorithms for Engineering Optimization. Retrieved from: https://www.lib.chalmers.se/

[69]   Solgi, R.M. (2020).
         https://pypi.org/project/geneticalgorithm/

[70]   SS-EN-ISO-14040:2006. Environmental management – Life cycle assessment – Principles and framework.

[71]   Zhang, Y., Lu, Yuehong, Huang, Zhijia, Chen, Demin, Cheng, Bo, Wang, Dong, Lu, Chengyu. (2025). Insight from Review Articles of Life Cycle Assessment for Buildings. *Applied Sciences*, *15 (14).* https://doi.org/10.3390/app15147751

[72]   SS-EN 15804:2012+A2:2019. Sustainability of construction works - Environmental product declarations - Core rules for the product category of construction products. *Swedish Institute for Standards*.

[73]   SS-EN-15978:2011. (2011) Sustainability of construction works – Assessment of environmental performance of buildings – Calculation method.

[74]   Mart´ınez-Muñoz, D., Mart´ı , J. V., Yepes,V. (2020). Steel-Concrete Composite Bridges: Design, Life Cycle Assessment, Maintenance, and Decision-Making.
         https://doi.org/10.1155/2020/8823370

[75]   Mara, V., Haghani, R. , Sagemo,A. ,Storck , L., Nilsson, D. . (2013). Comparative study of different bridge concepts based on life-cycle cost analyses and life-cycle assessment.
         Retrieved from: https://research.chalmers.se/

[76]   European Commission. (2013) Sustainable steel-composite bridges in built environment (SBRI).
         https://doi.org/10.2777/50286

[77]   Cope, A., Bai, Q., Samdariya, A., Labi, S. (2011). Assessing the efficacy of stainless steel for bridge deck reinforcement under uncertainty using Monte Carlo simulation.
         http://dx.doi.org/10.1080/15732479.2011.602418

[78]   Safi, M., Sundquist, Hakan, Karoumi, Raid (2014). Life-Cycle Costing Integration with Bridge Management Systems. *Civil Engineering and Architecture*, *2 (1).*
         DOI: 10.13189/cea.2014.020102

[79]   Pascal, D. (2023). pypi.org.
         https://pypi.org/project/geneticalgorithm2

[80]   Jean-Paul, L., Manfred, A. Hirt. (2013). Steel Bridges Conceptual and Structural Design of Steel and Steel-Concrete Composite Bridges.
         https://doi.org/10.1201/b15429

[81]   EN1990. (2002). Eurocode - Basis of structural design.

[82]   EN1994-2. (2005). Eurocode 4 - Design of composite steel and concrete structures - Part 2: General rules and rules for bridges.

[83]   EN1991-2. (2002). Eurocode 1: Actions on structures - Part 2: Traffic loads on bridges.

[84]   EN1993-1-4. (2006). Eurocode 3 - Design of steel structures - Part 1-4: General rules - Supplementary rules for stainless steels.

[85]   SS-EN1993-1-4:2006/A1:2015. (2015). Design of steel structures – Part 1-4: General rules – Supplementary rules for stainless steels.

[86]   TSFS-2018:57. (2018). Transportstyrelsens föreskrifter och allmänna råd om tillämpning av eurokoder.

[87]   Nissan, A., Woldeyohannes, Yohannes (2022). Life Cycle Assessment and Life Cycle Cost for Composite Bridges - Stainless Steel Corrugated Web Girders vs. Carbon Steel Flat Web Girders. *Chalmers University of Technology*.
Retrieved from: https://odr.chalmers.se/

[88]   Hlal, F. (2023). Stainless Steel Corrugated Web Girders for Composite Road Bridges: Concept Evaluation and Flange Buckling Resistance. *Chalmers University of Technology. Technical Report No ACE 2023:9*.
https://research.chalmers.se/publication/536891

[89]   Fu-siang, S. (2021). Comparative life cycle analysis for bridges made of conventional steel and stainless steel in the early design phases. *Chalmers University of Technology*.
Retrieved from: https://odr.chalmers.se/

[90]   Wallbaum, H. (2021). Life Cycle Cost Assessment (LCCA). *Chalmers University of Technology*.

[91]   Safi, M. (2013). Life-Cycle Costing: Applications and Implementations in Bridge Investment and Management. *Doctoral Thesis, KTH Royal Institute of Technology*.
Retrieved from: https://www.diva-portal.org/

[92]   Collin, P., Nilsson, Martin, Häggström, Jens (2011). International Workshop on Eurocode 4-2, Composite Bridges. *Technical report, Luleå University of Technology*.

[93]   Rossi, B., Marquart, S., Rossi, G. (2017). Comparative life cycle cost assessment of painted and hot-dip galvanized bridges. *Journal of Environmental Management*, *197*, 41-49.
https://doi.org/10.1016/j.jenvman.2017.03.022

[94]   Jáger, B., Kövesdi, Balázs, Dunai, László. (2017). Flange buckling resistance of trapezoidal web girders: Experimental and numerical study. EUROSTEEL 2017 *1 (2-3)*. 4088-4097. https://doi.org/10.1002/cepa.465

[95]   Drebenstedt, K., Euler, M. (2018). Statistical Analysis of Fatigue Test Data according to Eurocode 3. *Maintenance, Safety, Risk, Management and Life-Cycle Performance of Bridges, Melbourne. Leiden: CRC Press*, 2244–2251.

[96]   Anami, K., Sause, R., Abbas, H. (2005). Fatigue of web-flange weld of corrugated web girders: 1. Influence of web corrugation geometry and flange geometry on web-flange weld toe stresses. *International Journal of Fatigue*, *27 (4)*. 373-381. https://doi.org/10.1016/j.ijfatigue.2004.08.006

[97]   EN1993-1-5:2020(E). Eurocode 3 : Design of steel structures Part 1-5 : Plated structural elements.

[98]   Graciano, C., Flansbjer, M., Al-Emrani, M., Amani, M., Casanova, E. (2025). Experimental and numerical investigation on stainless steel corrugated girders subjected to patch loading. *Engineering Structures*. https://doi.org/10.1016/j.engstruct.2025.120221

[99]   Luo, R., Edlund, B. (1996). Ultimate strength of girders with trapezoidally corrugated webs under patch loading. *Thin-Walled Structures*. https://doi.org/10.1016/0263-8231(95)00029-1

[100]   Kövesdi, B., Braun, B., Kuhlmann, U., Dunai, L. (2010). Patch loading resistance of girders with corrugated webs. *Journal of Constructional Steel Research*. https://doi.org/10.1016/j.jcsr.2010.05.011

[101]   SÆMUNDSSON, D., INGÓLFSDÓTTIR, S. (2021). Nonlinear finite element analysis of stainless steel corrugated web girders subjected to patch loading. *Chalmers University of Technology*. Retrieved from: https://odr.chalmers.se/
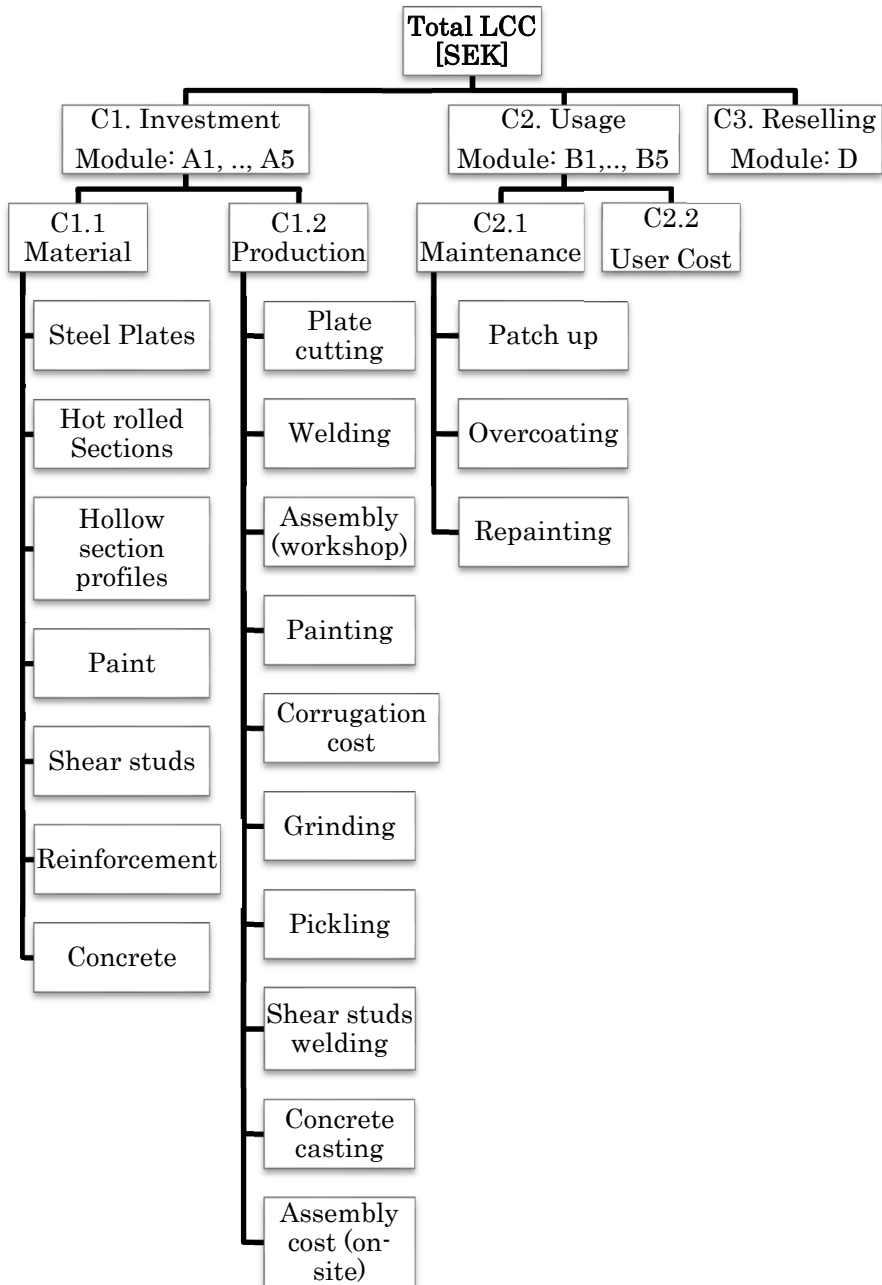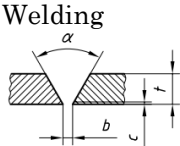
Appendix

Figure 35 An overview of the life cycle modules included in LCC

Table 13 Life cycle cost calculations

#	Item	Description
	Total LCC	Total LCC = Investment cost (C1) + Usage cost(C2) − Revenues from reselling (C3)
C1	Investment cost	Investment cost (C1) = Material cost(C1.1) + Production cost(C1.2)
C1.1	Material cost	Material cost = Main girders + Concrete + Reinforcement + Cross beams + Paint + Shear studs
	Production cost	Production cost = Plate cutting + Welding + Assembly (workshop) + Painting (for carbon steel) + Corrugation cost + Edge grinding to P3 + Pickling cost (for stainless steel) + Shear studs welding + Concrete casting + Assembly cost (on-site)
	Cutting cost	Cutting edges cost = 1650 SEK /ton of steel in the bridge
C1.2	Welding 	Welding cost = $ns * \text{L} * c_w/(l)$ ns: number of weld passes required for weld area $$ns = \frac{(A_w + 30)}{19}$$ A_w: the welding area for fillet or butt weld $[mm2]$ c_w: the welding cost per hour SEK/h l: the length that a welder runs per one hour (one pass), $or\ welder\ productivity$ L: the welding length $[m]$. Additional cost for butt weld: Edge preparation = 350 SEK / m of butt weld t > 20 mm Edge preparation = 200 SEK / m of butt weld t =< 20 mm
	Assembly cost (workshop)	Assembly cost = 30% ∗ Welding cost
	Painting	Painting cost = Painting area ∗ Painting unit cost Painting unit cost: Workshop: $C4 = 800\,SEK\,/m^2$ $C5 = 1000\,SEK\,/m^2$ On-site $C4 = 2400\,SEK\,/m^2$ $C5 = 3000\,SEK\,/m^2$

	Corrugation cost	Corrugation cost = Corrugation length * Corrugating unit cost Corrugating unit cost = 2000 SEK/m
	Grinding cost	Grinding cost = Grinding length * Grinding unit cost Grinding unit cost = 125 SEK/m This applied only to carbon steel
	Pickling cost	Pickling cost = Pickling area * Pickling unit cost Pickling unit cost = $300\ SEK/m^2$ This applied only to stainless steel
	Shear studs	Shear studs welding = Number of shear studs* Welding cost per piece Welding cost per piece = 45 SEK / piece
	Concrete casting	Concrete casting = Concrete volume * Casting unit cost Casting unit cost = 35 SEK/m3
	Assembly cost (on-site)	Assembly cost =Weld main girders to end cross beams+ weld main girders splices + bolt intermediate cross beams to the main girders Main girders and end cross beams (welded) = 9000 SEK / splice (= 16 manhours) Intermediate cross beams (bolted) = 2200 SEK /cross beam
C2	Usage cost	Usage cost (C2) = Maintenance activities cost (C2.1) + User cost (C2.2)
C2.1	Maintenance	Maintenance activities cost $$= \sum_{j} \left(\sum_{a} \left(A_{a,j} * P * C_{a,j} \right) \right) * (1 + i/1 + d)^n$$ $A_{a,j}$: The process for component j is needed for maintenance activity a. In this study, it refers to the initial painting area $[m^2]$ P: The operating percentage for each maintenance activity, i.e., patch-up, overcoating, and repainting [%] $C_{a,j}$: The unit cost of maintenance activity a, for component j $[\frac{SEK}{m^2}]$ i: The inflation rate [-] d: The discount rate [-] n: The year number [-]
C2.2	User Cost	User cost =

$$\sum_j \left(\sum_a \left(\text{Time} * \text{ADT} * T_{a,j} \right. \right.$$
$$\left. \left. * \left(h_t * p_t + h_p * (1 - p_t) \right) \right) \right) * (1 + i/1 + d)^n$$

Where Time $= L_{aff} * (1/v_r - 1/v_n)$

L_{aff}: Affected road length [km]

ADT: Average daily traffic [Vehicle per day]

$T_{a,j}$: The time needed for maintenance activity a, for component j [days]

h_t: Cost for heavy truck per hour [SEK/hour]

p_t: Heavy vehicles percent among the average number of daily traffic [%]

h_p: Cost for passenger car per hour [SEK/hour]

v_r: Reduced speed [km/hour]

v_n: Normal speed [km/hour]

C3 Reselling

Revenues from reselling =

$$\sum_j \left(\sum_m \left(q_{m,j} * r_m * P_{eol} \right) \right) * (1 + i/1 + d)^Y$$

$q_{m,j}$: The quantity of material m in component j [kg]

r_m: The recycling rate of material m [%]

P_{eol}: The unit price of end-of-life material m: [SEK/kg]
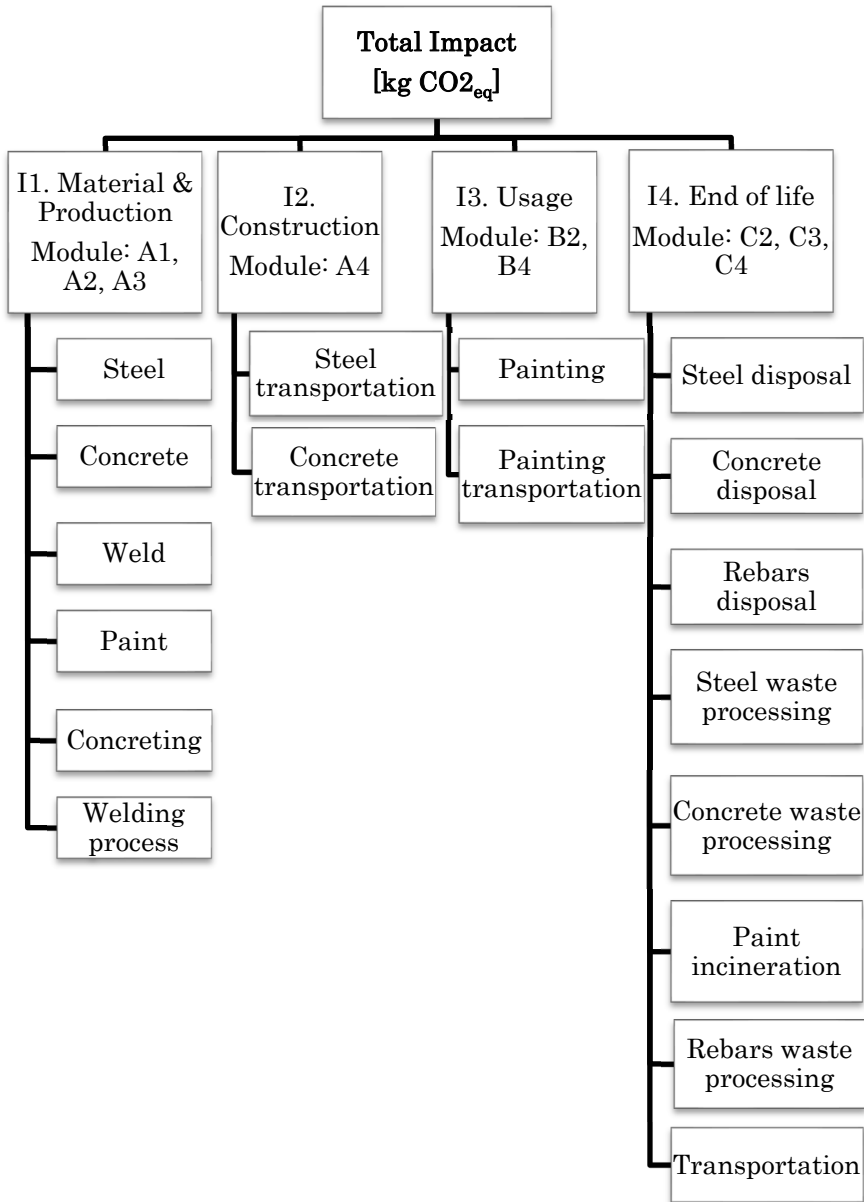
Y: The service life of the bridge [years]

Figure 36 An overview of the life cycle modules included in LCA

Table 14 Life cycle environmental impact calculations

#	Item	Description
	Total environmental impact	$Total\ Imapct\ =\ Production\ phase\ impact\ (I1)$ $+\ Construction\ phase\ impact(I2)$ $+\ Usage\ phase\ impact(I3)$ $+\ EOL\ impact(I4)$
I1	Production phase impact	$Production\ phase\ impact\ [kg\ CO2_{eq}]$ $=\ Material\ quantitiy\ [kg]$ $*\ material\ unit\ impact\ [kg\ \frac{CO2_{eq}}{kg}]$ *Material unit impact inlude material supply and the impact of additional processes needed in the production phase*
I2	Construction phase impact	$Construction\ phase\ impact\ [kg\ CO2_{eq}]$ $=\ Material\ quantity\ [kg]$ $*\ transport\ distance\ of\ material\ [km]$ $*\ The\ impact\ assessment\ results\ per\ (ton$ $*\ km)\ of\ the\ transportation\ [kg\ \frac{CO2_{eq}}{ton*km}]$
I3	Usage phase impact	$Usage\ phase\ impact\ [kg\ CO2_{eq}]$ $=\ Impact\ of\ paint\ production\ for\ the\ maintenance\ plan\ [kg\ CO2_{eq}]$ $+\ Impact\ of\ transportation\ of\ produced\ material\ for\ the\ maintenance\ activities\ [kg\ CO2_{eq]}$
I4	End-of-life (EOL) phase impact	$End-of-life\ phase\ impact\ [kg\ CO2_{eq}] =\ Impact\ of\ waste\ processing\ [kg\ CO2_{eq}]$ $+\ Impact\ of\ disposal\ processes\ [kg\ CO2_{eq}]$ $+\ Impact\ of\ transportation\ in\ the\ EOL\ phase\ [kg\ CO2_{eq}]$ $Impact\ of\ waste\ processing\ [kg\ CO2_{eq}]$ $=\ quantity\ of\ material\ [kg]*recycle\ rate$ $*\ impact\ assessment\ results\ per\ treatement\ process$ $of\ material\ [kg\ \frac{CO2_{eq}}{kg}]$ $Impact\ of\ disposal\ processes\ [kg\ CO2_{eq}]$ $=\ quantity\ of\ material\ [kg]*(1-recycle\ rate)$ $*\ impact\ assessment\ results\ per\ disposal\ material$ $[kg\ \frac{CO2_{eq}}{kg}]$ $Impact\ of\ transportation\ in\ the\ EOL\ [kg\ CO2_{eq}]$ $=\ quantity\ of\ material\ [ton]$ $*\ transport\ distance\ from\ construction\ site\ to\ landfills\ [km]*\ impact\ of\ transportation$ $in\ the\ EOL\ phase\ [kg\ \frac{CO2_{eq}}{ton*km}]$

Table 15 Design optimization results ID1-ID4

ID	ID1	ID2	ID3	ID4
Objective	LCC	Weight	LCA	Investment
Material grade	S355	S355	S355	S355
Span length [m]	52	52	52	52
N_{obs}	50000	50000	50000	50000
ADT	200	200	200	200
Allowable height [m]	3	3	3	3
Painting schedule	TRV	TRV	TRV	TRV
Weight [kg]	83,901	75,422	75,920	80,051
Investment cost [SEK]	3,290,301	3,325,363	3,320,511	3,282,455
LCC [SEK]	4,324,213	4,538,530	4,539,065	4,427,557
LCA [kg CO2$_{eq}$]	240,302	226,988	227,953	234,517
Paint during production [SEK]	835,956	975,504	978,435	922,022
Paint during usage [SEK]	1,059,077	1,235,620	1,241,169	1,169,032
Total painting [SEK]	1,895,033	2,211,124	2,219,604	2,091,054

Table 16 Design optimization results ID5-ID8

ID	ID5	ID6	ID7	ID8
Objective	LCC	Weight	LCA	Investment
Material grade	Duplex	Duplex	Duplex	Duplex
Span length [m]	52	52	52	52
N_{obs}	50000	50000	50000	50000
ADT	200	200	200	200
Allowable height [m]	3	3	3	3
Painting schedule	-	-	-	-
Weight [kg]	57,242	55,526	58,607	57,285
Investment cost [SEK]	3,413,809	3,392,586	3,463,928	3,448,910
LCC [SEK]	3,296,227	3,278,535	3,343,542	3,331,248
LCA [kg CO2$_{eq}$]	203,506	200,537	205,892	203,627
Paint during production [SEK]	-	-	-	-
Paint during usage [SEK]	-	-	-	-
Total painting [SEK]	-	-	-	-

Table 17 Design optimization results ID9-ID12

ID	ID9	ID10	ID11	ID12
Objective	LCC	LCC	LCC	LCC
Material grade	S355	Duplex	S355	S355
Span length [m]	52	52	52	52
N_{obs}	50000	500000	500000	500000
ADT	200	11000	11000	50000
Allowable height [m]	3	3	3	3
Painting schedule	Rossi	-	Rossi	Rossi
Weight [kg]	92,563	62,572	98,946	93,298
Investment cost [SEK]	3,394,852	3,698,384	3,491,677	3,490,909
LCC [SEK]	5,794,518	3,569,860	6,024,000	7,005,117
LCA [kg CO2eq]	259,652	212,864	269,693	261,124
Paint during production [SEK]	779,627	-	740,667	760,795
Paint during usage [SEK]	2,424,657	-	2,306,207	2,372,129
Total painting [SEK]	3,204,284	-	3,046,874	3,132,924

Table 18 Design optimization results ID13-ID16

ID	ID13	ID14	ID15	ID16
Objective	LCC	LCC	LCC	LCC
Material grade	S355	S355	S355	Duplex
Span length [m]	52	52	52	52
N_{obs}	500000	500000	500000	500000
ADT	11000	11000	11000	11000
Allowable height [m]	3	1.5	1.8	1.5
Painting schedule	TRV	TRV	TRV	-
Weight [kg]	82,021	118,638	103,868	95,098
Investment cost [SEK]	3,317,086	3,778,649	3,589,009	4,756,487
LCC [SEK]	4,457,183	4,800,917	4,752,973	4,561,115
LCA [kg CO2eq]	237,242	296,624	273,320	269,581
Paint during production [SEK]	845,547	762,762	868,967	-
Paint during usage [SEK]	1,070,473	964,363	1,101,329	-
Total painting [SEK]	1,916,020	1,727,125	1,970,296	-

Table 19 Design optimization results ID17-ID20

ID	ID17	ID18	ID19	ID20
Objective	LCC	LCC	LCC	LCC
Material grade	Duplex	S355	Duplex	S355
Span length [m]	52	52	52	30
N_{obs}	500000	125000	125000	50000
ADT	11000	5000	5000	200
Allowable height [m]	1.8	3	3	2
Painting schedule	-	TRV	-	TRV
Weight [kg]	79,036	81,329	56,683	31,411
Investment cost [SEK]	4,229,292	3,324,558	3,440,962	1,499,199
LCC [SEK]	4,066,935	4,513,031	3,324,537	1,949,521
LCA [kg $CO2_{eq}$]	241,577	236,557	202,564	110,853
Paint during production [SEK]	-	923,571	-	361,660
Paint during usage [SEK]	-	1,170,954	-	458,660
Total painting [SEK]	-	2,094,525	-	820,320

Table 20 Design optimization results ID21-ID25

ID	ID21	ID22	ID23	ID24	ID25
Objective	LCC	LCC	LCC	LCC	LCC
Material grade	S355	S355	Duplex	Duplex	Duplex
Span length [m]	30	30	30	30	30
N_{obs}	125000	500000	50000	125000	500000
ADT	5000	11000	200	5000	11000
Allowable height [m]	2	2	2	2	2
Painting schedule	TRV	TRV	-	-	-
Weight [kg]	34,235	32,785	24,691	23,551	26,164
Investment cost [SEK]	1,521,438	1,568,913	1,656,142	1,608,615	1,726,161
LCC [SEK]	2,006,733	2,138,804	1,605,433	1,560,251	1,672,428
LCA [kg $CO2_{eq}$]	115,520	112,940	102,898	100,915	105,486
Paint during production [SEK]	356,325	381,922	-	-	-
Paint during usage [SEK]	452,675	484,484	-	-	-
Total painting [SEK]	809,000	866,406	-	-	-